scientific reports

Check for updates

OPEN

A next-generation system for smoke inhalation integrated with a breathing lung-on-chip to model human lung responses to cigarette exposure

Arunima Sengupta[1,2]✉, Saskia Schmid[1,2], Noémie Grangier[2], Aurélien Dorn[1,2], Marco Hebestreit[3], Andreas Hugi[4], Kristína Žajdlíková[5,6], Anja Herbst[7,8], Paula Losada-Oliva[9], Heidi Ortolf-Wahl[3], Philippe Krebs[7], Janick D. Stucki[4], Vera van der Velpen[5,6], Jesus Perez-Gil[9], Tobias Krebs[3], Nina Hobi[4,10] & Olivier T. Guenat[1,10]✉

Continuous exposure to cigarette smoke (CS) significantly contributes to the development and progression of chronic obstructive pulmonary disease (COPD) and lung cancer. Animal models that inhale smoke nasally and have different lung physiology from humans may not accurately replicate cigarette smoke-induced health effects. Furthermore, traditional in vitro models fail to replicate the lung's dynamic mechanical forces and realistic inhalation exposure patterns, limiting their relevance in preclinical research. Here, we introduce an advanced smoke inhalation-based lung-on-chip system, the Continuous Flow AX12 (CFAX12), to investigate CS-induced cellular responses in a physiologically relevant manner. Unlike previous technologies, the CFAX12 integrates cyclic mechanical stretch with controlled whole-smoke exposure, allowing for a more accurate recreation of CS-induced alveolar microenvironment dynamics and barrier integrity responses. Using human alveolar epithelial cells, lung microvascular endothelial cells, and macrophages in mono- and co-culture models under air–liquid interface (ALI) conditions with breathing-like stretch (Str), we simulated key lung microenvironment features. Our results show that CS exposure using the CFAX12 induced a ~ 60% reduction in trans-barrier electrical resistance (TER), increased ROS generation depending on cellular model complexity, and a ~ 4.5-fold increase in IL-8 gene expression, all key hallmarks of early COPD pathogenesis. These findings underscore smoke-induced epithelial damage, inflammation, and oxidative stress, all of which contribute to alveolar barrier dysfunction and disease progression. Also, CFAX12 provides a more physiologically relevant alternative to submerged cigarette smoke extract (CSE) treatments, offering controlled whole-smoke exposure using the VC10 Smoking Robot, ensuring precisely regulated smoke delivery. Additionally, inclusion of pulmonary surfactant reduced IL8 gene levels by ~ 5 folds. Hence, by integrating mechanical and biological complexity, CFAX12 offers a robust platform for assessing inhaled smoke effects and identifying therapeutic targets. It's application in COPD drug screening can facilitate the discovery of compounds that preserve alveolar integrity, reduce inflammation, and mitigate oxidative damage, ultimately bridging the gap between regulatory and preclinical research applications.

Keywords Lung-on-chip, Inhalation, Cigarette smoke, Stretch, Air–liquid interface, Alveolar toxicity, CSE

[1]Organs-On-Chip Technologies, ARTORG Center for Biomedical Engineering, University of Bern, Bern, Switzerland. [2]Alexis Technologies AG, Bern, Switzerland. [3]VITROCELL Systems GmbH, Waldkirch, Germany. [4]Swiss Organs-On-Chip Innovation, AlveoliX AG, Bern, Switzerland. [5]Clinical Pharmacology and Toxicology, Department of General Internal Medicine, Inselspital, Bern University Hospital, University of Bern, Bern, Switzerland. [6]Institute of Pharmacology, University of Bern, Bern, Switzerland. [7]Institute of Tissue Medicine and Pathology, University of Bern, Bern, Switzerland. [8]Graduate School for Cellular and Biomedical Sciences, University of Bern, Bern, Switzerland. [9]Department of Biochemistry, Faculty of Biology, and Research Institute "Hospital 12 de Octubre (i+12)", Universidad Complutense, Madrid, Spain. [10]These authors contributed equally: Nina Hobi and Olivier T. Guenat. ✉email: arunima.sengupta@unibe.ch; olivier.guenat@unibe.ch

Chronic lung conditions like COPD and lung cancer are leading causes of morbidity and mortality worldwide, with cigarette smoke (CS) being the primary risk factor for these fatal conditions[1,2]. COPD is a progressive disease characterized by chronic airway inflammation and alveolar remodeling. COPD encompasses various severe manifestations, including emphysema, which is characterized by irreversible alveolar remodeling, resulting in impaired gas exchange and respiratory dysfunction[3]. Chronic exposure to CS manifests as pathological changes like heightened oxidative stress, increased lung permeability, loss of tight junctions, epithelial-mesenchymal transition (EMT) all of which contributes to tissue destruction and impaired lung function[4–6]. Functionally, alveolar macrophages in emphysematous lungs exhibit dysregulated cytokine release, driving chronic inflammation and further amplifying epithelial damage (Kapellos et al. 2018). Additionally, the altered lipid metabolism disrupts surfactant homeostasis, further impairing lung function[7,8]. The human alveolar microenvironment consists of tightly regulated crosstalk between epithelial, endothelial, and immune cells, which is critical for maintaining lung homeostasis and responding to external insults such as CS[9]. In vivo, alveolar macrophages (AMs) serve as frontline immune cells, interacting directly with epithelial and endothelial cells to regulate inflammation, phagocytosis, and extracellular matrix remodeling. A recent insert-based lung model incorporating epithelial-alveolar macrophage co-cultures have demonstrated that macrophages modulate epithelial cell function under cigarette smoke exposure, mimicking in vivo inflammatory dynamics and macrophage polarization shifts[10]. Furthermore, endothelial cells play a crucial role in maintaining the air-blood barrier and regulating inflammatory signaling in response to inhaled toxicants[11]. These findings emphasize the necessity of co-culture models in studying complex cellular interactions and disease progression, enhancing the translational value of in vitro lung-on-chip models for inhalation toxicology research (Fig. 1).

Despite significant advancements in our understanding of COPD, the complex molecular mechanisms underlying CS-induced lung damage remain incompletely understood. Existing animal models have limitations in replicating COPD exacerbations from cigarette smoke. Common laboratory animals, like mice and rats, are obligate nose-breathers, making them poor representatives of human respiratory exposure[12,13]. This raises concerns about their applicability in smoke exposure studies. Additionally, increasing societal and legislative pressure, including the FDA Modernization Act of 2021 and the Humane Research and Testing Act, is driving efforts to reduce animal testing. Alternatives are needed due to high costs, time constraints, and the frequent failure of animal data to translate to human clinical trials[14,15]. Current regulatory frameworks for tobacco and nicotine-containing products (TNCPs) are strongly emphasizing standardized, high-throughput in vitro models with toxicologically relevant endpoints[16]. While early research provided a strong foundation, it was largely exploratory and not designed for risk assessment applications. With the shift toward new approach methodologies (NAMs) to replace animal testing, there is a growing need for reproducible, physiologically relevant models that align with evolving requirements. Advancing these models through interdisciplinary collaboration will be essential for generating robust toxicological data suitable for risk evaluation and decision-making.

Further, a critical limitation of most traditional in vitro existing smoke models is their reliance on the use of cigarette smoke extract (CSE) rather than whole cigarette smoke (CS). CSE, which simplifies the exposure process by focusing on hydrophilic constituents, does not fully represent the complex mixture of chemicals and particulate matter found in whole cigarette smoke[17,18]. Whole CS, inhaled into the respiratory system, is a complex mixture of chemicals, including solid/liquid droplets in a gaseous phase generated by burning and pyrolysis processes, with fresh mainstream smoke containing approximately 4,700 identified substances[19,20]. Additionally, traditional in vitro models often treat lung cells with CSE under submerged conditions, rather than at the air–liquid interface, an important physiological aspect of the air-blood barrier environment. Moreover, the preparation of CSE involves multiple protocols that lack standardization, resulting in significant inter-laboratory variations in the observed effects of CSE treatments[21]. Hence, such study fails to reproduce the physiological inhalation and delivery of smoke to lung tissue and lacks robustness. Consequently, the scarcity of human-relevant preclinical models significantly contributes to high therapeutic failure rates resulting in fewer effective drugs for treating COPD patients and ultimately to rising healthcare costs[22]. The advent of microfluidic technology and the development of organ-on-chip systems have provided new avenues for creating more physiologically relevant in vitro systems. Lung-on-chip models offer the capability to mimic the dynamic environment of the human lung, including ALI conditions, cyclic mechanical breathing-like stretch, flow, topography, co-culture of different cell types[23,24]. Such advanced models are being utilized in preclinical safety profiling of therapeutics[25] and can be even combined with advanced aerosol inhalation systems[26] for toxicology and risk assessment studies. These features enable a more accurate representation of the lung's microenvironment, allowing for real-time study of cellular responses to cigarette smoke.

Only a few studies on cigarette smoke inhalation using microfluidic cell culture systems have been reported so far[27]. A notable early study by Benam et al.[28,29] utilized a lung-on-chip model to expose bronchial epithelial cells to cigarette smoke, leading to the identification of ciliary micro-pathologies induced by cigarette and e-cigarette exposure. However, while valuable, this model had key limitations, including a lack of reproducible smoke dose delivery, the inability to assess cigarette smoke-induced toxicity in the distal lung, and the absence of essential readouts like trans-barrier electrical resistance (TER), restricting its applicability for studying alveolar-level injuries. Similarly, a more recent study by Lagowala et al.[11] combined transwell co-culture systems, precision-cut lung slices (PCLS), and a membrane-free lung-on-a-chip model to investigate epithelial-immune interactions and chronic smoke-induced lung remodeling. While this model provided detailed imaging and immune cell incorporation, they lacked TER assessment as well, and biomechanical stretch, limiting their ability to fully replicate inhalation-induced alveolar dysfunction. Additionally, the design of the smoking robot plays a critical role in experimental accuracy, as valve systems within smoke-generating components can interact with cigarette smoke, potentially altering its chemical composition. To overcome these challenges, we employed the VC10 Smoking Robot (Vitrocell Systems, Germany), which is well-characterized and optimized for in vitro studies[30].

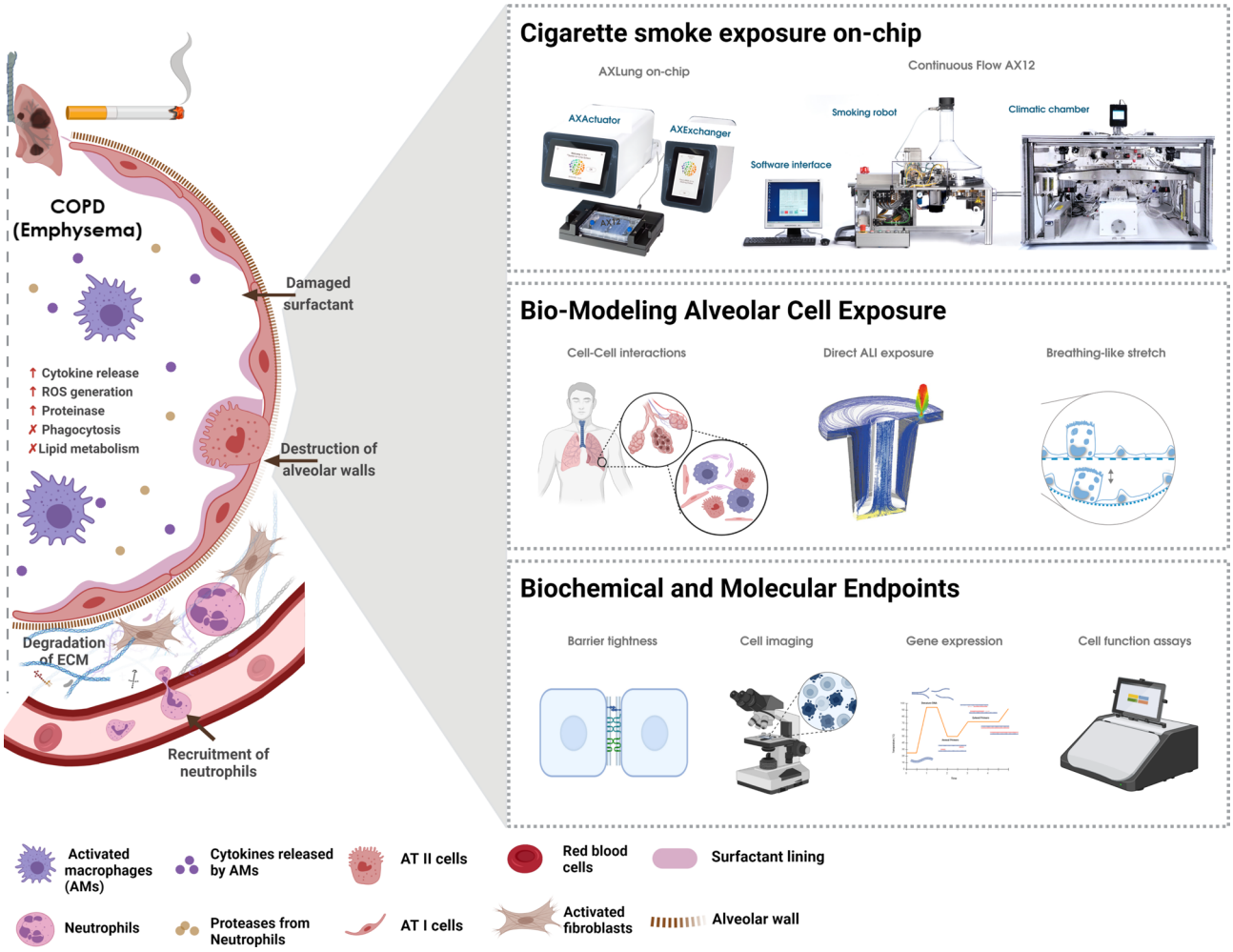

Fig. 1. Critical role of the lung microenvironment in mediating the effects of cigarette smoke on alveolar health. (Left) Schematic representation of cellular and molecular alterations in the alveolar region due to CS exposure, illustrating key processes such as cytokine release, reactive oxygen species (ROS) generation, increased protease activity, phagocytosis, altered lipid metabolism, degradation of the extracellular matrix (ECM), and recruitment of neutrophils. Various cell types, including activated macrophages (AMs), neutrophils, alveolar type I (AT I) and type II (AT II) cells, and activated fibroblasts, are depicted in the context of emphysematous (COPD) damage. (Right top) Experimental setup used for cigarette smoke exposure, featuring the AX12 Lung-on-Chip system and Continuous Flow AX12 (CFAX12). (Right middle) Overview of the different exposure conditions employed in the study, including use of different cell types, air–liquid interface (ALI) exposure and physiological stretch conditions. (Right bottom) Summary of the key endpoints measured in the study, like barrier health, cellular morphology via imaging, gene expression analysis to monitor changes at the molecular level and functional assays to evaluate cytotoxicity, ROS generation, and other cellular functions.

This system ensures controlled, reproducible smoke exposure in a physiologically relevant environment, allowing for precise regulation of exposure variables. Moreover, it reduces human error and limits direct exposure to harmful smoke constituents, enhancing the reliability and safety of smoke exposure experiments[31].

Among the few other existing microfluidic systems[32–34], the majority rely on submerged CSE treatments, which fail to mimic physiologically relevant air–liquid interface (ALI) conditions and dynamic mechanical forces present in the lung. These limitations underscore the need for a next-generation lung-on-chip system like CFAX12, which can more accurately replicate alveolar microenvironments and assess cigarette smoke toxicity in a reproducible and physiologically relevant manner.

The CFAX12 lung-on-chip platform overcomes these challenges by integrating key features that are not present in any other existing system. Unlike previous models, CFAX12 uniquely allows periodic TER measurements, providing a reproducible, non-invasive assessment of barrier integrity over time, a critical endpoint for inhalation toxicity studies. Additionally, the CFAX12 lung-on-chip platform is the only system to integrate biomechanical stretch, simulating breathing-like forces, which significantly influence cellular responses to cigarette smoke exposure. Furthermore, no other model to date has demonstrated such a high level of bio-model complexity, as our study highlights the importance of co-culture systems and the inclusion of macrophages in smoke exposure

models, which are essential for capturing the immune-inflammatory responses involved in COPD pathogenesis. This system includes the VC10 smoking robot that mimics human smoking behavior and delivers whole smoke to alveolar cells cultured under ALI and stretch conditions and a climatic chamber to house all the components under relevant physiological conditions. The use of human alveolar epithelial cells (^{AX}iAECs) in co-culture with endothelial cells (hLMVECs) and macrophages (THP-1 or primary blood-derived macrophages; pBDMs) enables a comprehensive assessment of cellular interactions and responses to smoke exposure. Here, we also investigated the differential impact of whole smoke exposure versus traditional CSE treatment in lung cells. Our results highlight the sensitivity of the epithelial barrier, oxidative stress, and inflammatory responses under dynamic breathing-like stretch conditions, underscoring the importance of mechanosensitive responses in smoke-induced lung damage. Additionally, the potential protective effect of pulmonary surfactant in mitigating smoke-induced damage was investigated. Given the critical need for physiologically relevant smoke exposure models of the alveolar space, the CFAX12 is developed as a platform for advancing inhalation toxicology research and assessing therapies aimed at reducing smoke-related lung damage.

Methods

CFAX12 for in vitro analysis of cigarette smoke effects on-chip

The Continuous Flow AX12 (CFAX12) exposure system was employed to investigate the effects of cigarette smoke on lung cells cultured in the AX12 Lung-on-chip (AlveoliX, Switzerland) (Fig. 2A). The system integrates a modified smoking machine (VC10, Vitrocell Systems, Germany) described earlier, which has been adopted for the current study to accommodate the AX12. Briefly, the smoke machine VC10 is connected to an exposure module housed within a climatic chamber, enabling precise control of environmental conditions during the experiments. The VC10 generates and delivers cigarette smoke to the exposure module. Cigarettes are automatically loaded from a magazine (Supplementary Fig. 1B) into the cigarette holder port (Fig. 2C, Supplementary Fig. 1F), where an electric lighter (Fig. 2D) ignited them. A syringe pump (Supplementary Fig. 1H), designed to mimic the inhalation process of a human smoker, drew puffs, and transferred the smoke to the dilution system (Supplementary Fig. 1C). The VC10 allows for adjustable puff parameters, including volume, duration, interval, and frequency. At the end of each smoking cycle, the butt extractor (Supplementary Fig. 1G) retracts all the burnt cigarettes and automatically dispenses them into an in-built ashtray. For this study, the Health Canada Intense (HCI) smoking regime was employed in terms of puff volume, duration, and number. Specifically, one 1R6F standard research cigarette (Kentucky Tobacco Research & Development Center, Lexington, KY, USA) was smoked per cycle (one cycle in total), with a puff volume of 55 mL, a puff duration of 2 s, a puff interval of 30 s, and a puff exhaust time of 8 s (Fig. 2B). A dilution airflow of 0.5L/min was applied, resulting in a dilution factor of 0.1803 (Dilution Factor = Volume of Smoke / (Volume of Smoke + Volume of Fresh Air). This standardized protocol facilitates the reproducibility and comparability of results. The exposure module was modified to house the AX12 lung-on-chip (Fig. 2E), which was maintained at a constant physiological temperature of 37 °C and humidity (~ 95%), achieved through the controlled environment of the climatic chamber assisted with additional humidification station (Supplementary Fig. 1A) attached with water baths (Supplementary Fig. 1D). The cigarette smoke generated by the VC10 smoking machine was diluted and homogenized with cigarette smoke-free air before being delivered to the exposure head. This setup ensures that the smoke reaches the cells cultured at the ALI condition in a controlled and uniform manner (Fig. 2G). The smoke delivery system included a series of flow controllers that regulated the air and smoke flow rates to achieve the desired dilution (Supplementary Fig. 1E). The exposure head, equipped with trumpet-shaped inlets, ensured even distribution of smoke over the cells. A vacuum pump generated a flow that directed the aerosol towards the cells, while the excess smoke was exhausted through an exhaust tube (Fig. 2F). The device was installed by the manufacturer and subsequently underwent Installation Qualification (IQ) and Performance Qualification (PQ) in accordance with their specifications at the time. Thereafter, performance was monitored daily through leakage tests and the assessment and adjustment of the puff volume. The CFAX12 system allowed for the precise adjustment of smoke concentration, simulating real-world smoking conditions. The exposure module featured two parallel aerosol channels, enabling simultaneous exposure to different conditions within the same experiment. Typically, one chip of the AX12 was exposed to cigarette smoke, while the other chip was exposed to clean air as a control. This setup provided a robust comparative analysis of smoke-induced effects versus healthy baseline conditions. Throughout the experiments, the system's software interface recorded and monitored all relevant parameters, including puff volume, duration, interval, and frequency.

Preparation of cigarette smoke extract

Cigarette smoke extract (CSE) was prepared utilizing the VC10 smoking robot component of the CFAX12. One 1R6F cigarette was loaded into the magazine which loaded it into the cigarette holder port. The smoke generated was drawn by a syringe pump, mimicking smoker inhalation, and delivered to a T-tube connected to a PBS-filled (10 ml) falcon tube. Smoke was bubbled through the PBS to create fresh 100% CSE extract before each experimental round. After completing the smoking cycle, the CSE was filtered using a 0.22 µm sterile filter and diluted with warm culture medium to the desired concentration (0%, 2.5%, 5%, 10%, 25%, 50% and 100%). The prepared CSE was then applied to the apical side of the cell cultures in the AX12 for subsequent experimental procedures.

^{AX}Lung on-chip technology

As described previously[35,36], the ^{AX}Lung-on-chip system (AlveoliX AG, Switzerland) comprises the Lung-on-chip (AX12) consumable (Fig. 2B), two electro-pneumatic devices (^{AX}Exchanger and ^{AX}Breather), and the interface platform (^{AX}Dock) (Fig. 1). Cell seeding and medium exchanges were performed according to the manufacturer's recommendations (AlveoliX AG). To initiate the breathing mechanism, the AX12 was positioned

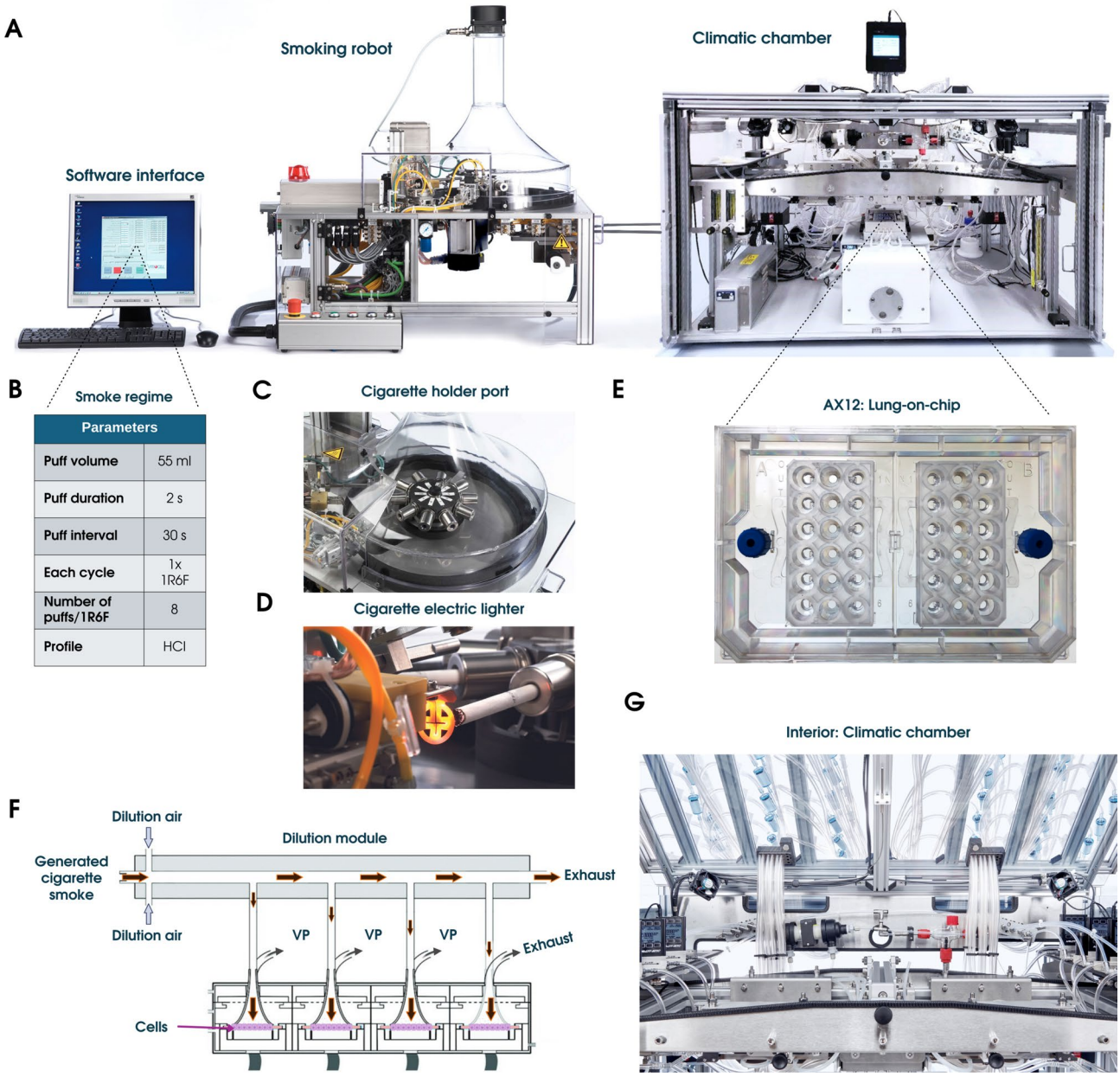

Fig. 2. Components of the CFAX12 System. (**A**) Overview of the three main elements of the CFAX12 (from left to right): the computer system with the software interface, the VC10 smoking robot and the Climatic chamber. (**B**) The operation is controlled via a software interface where the Health Canada Intense (HCI) smoking regime was selected. (**C**) The cigarettes are loaded into the cigarette holders fully automatically and without damage, with the rotation of the holder controlled by a stepper motor. (**D**) The electric lighter to ensure automatic and contactless ignition. (**E**) The lung-on-chip consumable, AX12. (**F**) The VC10 smoking robot initiates the process delivering the smoke to the dilution system, where dilution air is added to the smoke feed stream. The whole smoke dilutes in the dilution module, passes through the exposure head, and reaches the AX12 with the cells seeded, secured in the exposure module. A sample flow generated by a vacuum pump (VP) diverts the aerosol towards the cells via "trumpet" inlets, and after contacting the cells, the smoke exits through an exhaust tube; the continuous dilution air flow ensures that any remaining smoke is also exhausted. (**G**).

within the ^{AX}Dock inside the incubator. The three-dimensional (3D) cyclic stretch (10% linear strain, 0.2 Hz) was then initiated via a touchscreen control on the ^{AX}Breather, which deflected the microdiaphragm by generating negative cyclic pressure. Both stretch (Str) and non-stretched static conditions were run simultaneously on a single AX12, as the two chips were controlled independently.

Cell culture and treatment

The alveolar epithelial cell line (^{AX}iAECs) used in this study was procured from AlveoliX (Switzerland). These cells were derived from primary human alveolar epithelial cells (AECs) isolated from resected lung tissue and subsequently immortalized using InscreeneX's CI-Screen technology, as described by Lipps et al.[37]. The ^{AX}iAECs were cultured according to the manufacturer's instructions, as previously described and characterized by Sengupta et al.[35].

Human Lung Microvascular Endothelial Cells (hLMVECs) purchased from PromoCell were expanded in flasks using AX Endothelial Medium. hLMVECs were first seeded on the basolateral side of each membrane in the AX12 at a density of 106,000cells/cm^2, followed by a 2-h incubation, and then ^{AX}iAECs were seeded apically at a density of 409,000 cells/cm^2 on day 0 for all co-culture experiments. The cells were maintained at 37 °C, 5% CO2, with the medium replaced every 2 days. On the AX12, ^{AX}iAECs were maintained in AX Alveolar Epithelial Barrier Medium (AlveoliX, Switzerland) supplemented with 1% penicillin–streptomycin (Thermo Fisher Scientific, Switzerland) for mono-culture studies and ^{AX}iAECs/hLMVECs were maintained in AX E2 Alveolar Barrier Medium (provided by AlveoliX) for all dual-culture studies. In all studies, the ^{AX}iAECs alone or in co-culture with the hLMVECs were maintained and differentiated on the AX12 for three weeks prior to cigarette smoke treatment or exposure conditions, where ALI and stretch was initiated in specified experiments around 10 days prior to smoke exposure.

Human primary blood-derived monocytes (pBDMCs) were isolated from donor buffy coats using the EasySep™ Direct Human Monocyte Isolation Kit (Stemcell, #19669), which isolates primary CD14 + monocytes via negative immunomagnetic selection according to the manufacturer's protocol (Supplementary Fig. 2A). The pBDMCs were cultured in RPMI medium (21875-034, Gibco) with 10% FBS, 1% P/S, and 2 mM L-Glutamine for one day before being differentiated into macrophages (primary blood-derived macrophages; pBDMs) in the same medium supplemented with 50 ng/mL M-CSF (Peprotech, #300-25) for six days, with medium exchanges every 2 days. After six days, the cells were washed with PBS and detached using pre-warmed Accutase (Sigma Aldrich, # A6964). The pBDMs cell suspension was centrifuged, and the cell pellet was resuspended in fresh triple-culture medium (2 parts of AX E2 Alveolar Barrier Medium: 1part of RPMI) and added on the apical side at a ratio of 1:7 (pBDMs: ^{AX}iAECs). The usage of donor-derived pBDMCs was approved by the Blutspendezentrum (SRK Bern).

The THP-1 monocytes (ATCC; TIB-202) are an immortalized monocyte-like cell line derived from the peripheral blood of a patient with acute monocytic leukemia. These cells were cultured in RPMI medium (21875-034, Gibco) supplemented with 10% FBS, 1% P/S, and 2 mM L-Glutamine. Differentiation of THP-1 monocytes into macrophage-like cells was induced using 100 nM phorbol 12-myristate 13-acetate (PMA; Sigma) and incubated for 48 h following the established protocol by Kletting et al.[38]. After incubation, the differentiated THP-1 macrophages were allowed to rest in PMA-free medium for an additional 24 h prior to seeding in the AX12. For triple-culture experiments the THP1s were added apically at a ratio of 1:7 (THP-1: ^{AX}iAECs).

For all experiments conducted, unless specified otherwise, 0 h refers to the time point immediately before exposure to CS or CSE. The 4 h, 24 h, and 48 h time points indicate the number of hours post-exposure.

Both pBDMs and THP-1 macrophages were added to the epithelial/endothelial (^{AX}iAECs/hLMVECs) co-culture 5 days prior to CS exposure. All cell lines were routinely monitored for mycoplasma contamination using a mycoplasma detection kit (MycoStrip, InvivoGen).

Pulmonary surfactant

Porcine-derived pulmonary surfactant was added to the co-culture conditions 24 h before smoke exposure (Fig. 7A). Curosurf® (poractant-alpha, Chiesi Farmaceutici, Parma, Italy) is a clinical surfactant preparation provided as a suspension at 80 mg/mL containing more than 90% of surfactant phospholipids and around 1% by mass of surfactant proteins SP-B and SP-C. It was carefully diluted in 1X PBS (Sigma Aldrich, #D8537) to a concentration of 30 µg/µl and 5 µl was added on the apical side of the membrane per well in the AX12.

Flow cytometry analysis

Freshly isolated primary blood-derived monocytes (pBDMCs) were analyzed using flow cytometry. In brief, cells were incubated at 4 °C with the following antibodies: anti-CD45 (Biolegend, # 30-F11), anti-CD14 (Biolegend, # M5E2), as well as with Live Dead Fixable Blue (Thermofisher) for live/dead cell discrimination. After washing, samples were acquired using a LSRII SORP device (BD Bioscience, USA) and analyzed with the FlowJo software (version 10.8.1, BD Bioscience).

Liquid chromatography–mass spectrometry measurements

CS exposure was performed in the CFAX12, and smoke was trapped in 1 × PBS filled wells in the AX12. Nicotine, cotinine and 3'-hydroxy-cotinine (OH-cotinine) were measured in PBS using a quantitative liquid chromatography coupled to tandem mass spectrometry (LC–MS/MS) method, based on a previously validated method for saliva (as established in[39]). In brief, the measurements were performed using a Shimadzu Prominence HPLC (Shimadzu, Reinach, Switzerland) coupled to a SCIEX 4000 QTrap mass spectrometer (AB Sciex, Darmstadt, Germany) and a PAL autosampler (CTC Analytics, Zwingen, Switzerland). Chromatographical separation was achieved with an XBridge BEH C18 column (3.5 µm, 4.6 × 100 mm, 130 Å, Waters, Dättwil, Switzerland) and a delay column of the same specifications was used to minimize environmental contamination. Mobile phase A consisted of 0.01% NH4OH in water and mobile phase B of 0.01% NH4OH in methanol with a gradient starting at 5% mobile phase B which linearly increased to 90% B at 2 min and to 100% B at 2.5 min. The PBS samples were combined with 80% methanol containing the deuterated internal standards (IS) (25 µL sample + 250 µL IS mix). For quantitation, calibration curves were constructed from at least six consecutive calibrators in the range from 1 to 4000 ng/ml, covering the relevant concentration ranges in the samples. When

necessary, the samples were pre-diluted 10 × with 80% MeOH to ensure concentrations within the dynamic range of the method. The lower limits of quantification (LLOQs) of the method were 2, 1 and 1 ng/mL for nicotine, cotinine and 3'-OH-cotinine, respectively.

TER measurement

To determine barrier formation, trans-barrier electrical resistance (TER) measurements were taken every two days, starting 48 h after cell seeding as discussed previously[35]. In brief, a commercially available 96-well plate electrode (STX100MC96, World Precision Instruments) and an Epithelial Volt/Ohm Meter (EVOM3; World Precision Instruments) was used. TER was measured in mono, and co-culture conditions until endpoint. Before taking a reading, the electrodes were carefully sterilized using 70% v/v ethanol for 5 min and then rinsed in distilled water for another 5 min at room temperature (RT). The "TER measurement" option was initiated on the ^{AX}Exchanger while taking readings. For cells kept in ALI, pre-warmed 1X sterile PBS was added 15 min prior to the measurements and then later re-equilibrated after TER readings. The background TER (Ohm) data was obtained from a well having no cells. For analysis, the background subtracted TER (Ohm) values were multiplied by the surface area of each cell culture well (0.071 cm^2 in AX12) to obtain the final TER reading in $Ohm.cm^2$.

qRT-PCR

Total RNA was isolated separately from the apical and basal chamber and subsequently purified using the Direct-zol™ RNA Microprep kit (Zymo Research, Switzerland) using the manufacturer protocol. Purity and concentration of RNA was analyzed using a Nano-Drop Spectrophotometer (Thermo Fischer Scientific, Switzerland). Next, cDNA was transcribed using the Super Script III Reverse Transcriptase kit (Life Technologies, Switzerland). Finally, qRT-PCR reactions were performed in triplicates with SYBR® Select Master Mix (Thermo Scientific) in an ABI7500 Fast (Applied Biosystems) real-time qRT-PCR system. Target gene expression was normalized to housekeeping gene expression (GAPDH). The primer sequences are provided in supplementary Table 1.

ELISA

IL8 ELISA was performed with a human IL8 ELISA kit (BioLegend, #431504), according to the manufacturer's instructions. All ELISA experiments were repeated in technical duplicates with apical supernatants collected from the AX12 Lung-on-chip.

LDH cytotoxicity assay

Collected apical supernatants from individual AX12 wells were analyzed for Lactate Dehydrogenase (LDH) release. The LDH-Glo cytotoxicity assay kit (Promega, #J2381) was used according to the manufacturer's protocol. All LDH experiments were repeated in technical duplicates. The respective cell culture medium was taken as the "blank" control. Healthy untreated cells were considered as "negative" control for the assay, whereas cells treated with 1% Triton X-100 were considered as the "positive" control for maximum LDH release. Luminescence was measured using a microplate reader (Tecan Reader M1000).

Measurement of ROS activity

To measure reactive oxygen species (ROS) from smoke exposed cells, the DCFDA/H2DCFDA cellular ROS assay kit (Abcam; ab113851) was used according to the manufacturer's instructions. A blank or negative control (well with no cells) was included to normalize the background for subtraction. A positive maximal ROS control was prepared with Ter-butyl hydrogen peroxide (TBHP) at a concentration of 150 µM in buffer (provided within the kit). DCF amount obtained from the cells was then finally detected at Ex/Em = 485/535 nm in a fluorescence microplate reader (Tecan Reader M1000).

Immunofluorescence staining and imaging

Cells in AX12 were fixed using 4% paraformaldehyde in distilled PBS- (PBS without calcium and magnesium). "Medium exchange" function on the ^{AX}Exchanger was used to fix the cells within the basal chamber. Chips from the AX12 were unscrewed and opened using the ^{AX}Disassembly tool (AlveoliX, Switzerland) prior to staining and mounting. Cells were first permeabilized using 0.1% Triton X-100 (Sigma-Aldrich, Germany) dissolved in PBS for 15 min at RT and then blocking buffer (2% BSA in sterile PBS) was added. The cells were incubated for 1 h at RT with the blocking buffer. The antibodies used for the study are conjugated Alexa Fluor 488 anti-ZO1 (Thermo Fischer Scientific, #339188) and conjugated Alexa Fluor 568 anti-CD31/Pecam-1 (Cell Signaling; #61255). The antibodies were diluted in 2% BSA/PBS and incubated overnight at 4 °C. Nuclei were stained with Hoechst (1:1000 dilution; Invitrogen, #33342). The actin cytoskeleton was visualized using the conjugated Alexa Fluor 647 phalloidin stain (1:300 dilution; # PHDN1-A, Cytoskeleton, Inc.). Lastly, the stained membranes were sealed between two glass coverslips using a mounting medium (Sigma-Aldrich, #F6182). Images were obtained using a confocal laser scanning microscope (Zeiss LSM 980) using appropriate settings.

Statistical analysis

All bar graph data are presented as mean ± standard error of the mean (SEM) unless specified otherwise. For all AX12 experiments, "N" represents the experimental repetitions, and "n" represents the number of individual wells estimated for all experiments with mRNA and cell supernatants. All statistical tests were performed using t-tests, one-way or two-way analysis of variance (ANOVA) with p values adjusted for multiple comparisons using Tukey's multiple comparisons test, $*p < 0.0332$, $**p < 0.0021$, $***p < 0.0002$, $****p < 0.0001$. For all studies, the absence of statistical significance brackets indicated that the p-value was greater than 0.0332. GraphPad Prism software v10.0 was used for data analysis. The exact number of repeats performed for each experiment is indicated in the corresponding figure legends.

Results

Homogeneity of smoke exposure

To evaluate the homogeneity of cigarette smoke reaching the cells in the AX12, a series of dose distribution studies were conducted. These studies were designed to assess both the distribution of smoke within experimental rounds and within individual wells of the AX12 (Supplementary Fig. 3C). For this study, both Chip A and Chip B were exposed to cigarette smoke (Fig. 3A). The modular design of the exposure system allowed for the connection of either both channels with a U-piece to create identical conditions across all 12 wells of the AX12 (as shown in Fig. 3A) or have control air exposed on one chip and cigarette smoke on another chip within the same AX12 (as shown in Fig. 3D). Carbon dots, components of cigarette smoke with a strong fluorescence[40] were used as marker. The fluorescence intensity of the carbon dots deposited in each well was considered proportional to smoke deposition. The deposition values in three experimental rounds (N1, N2 and N3) were noted to be in range of ± 15% standard deviation validating uniform smoke distribution across different runs (Fig. 3B). To examine the intra-well dose distribution within the AX12, fluorescence intensity was used as an indicator (Relative Fluorescence Units, RFU). The heatmaps for each well position in Chip A and Chip B indicated a high

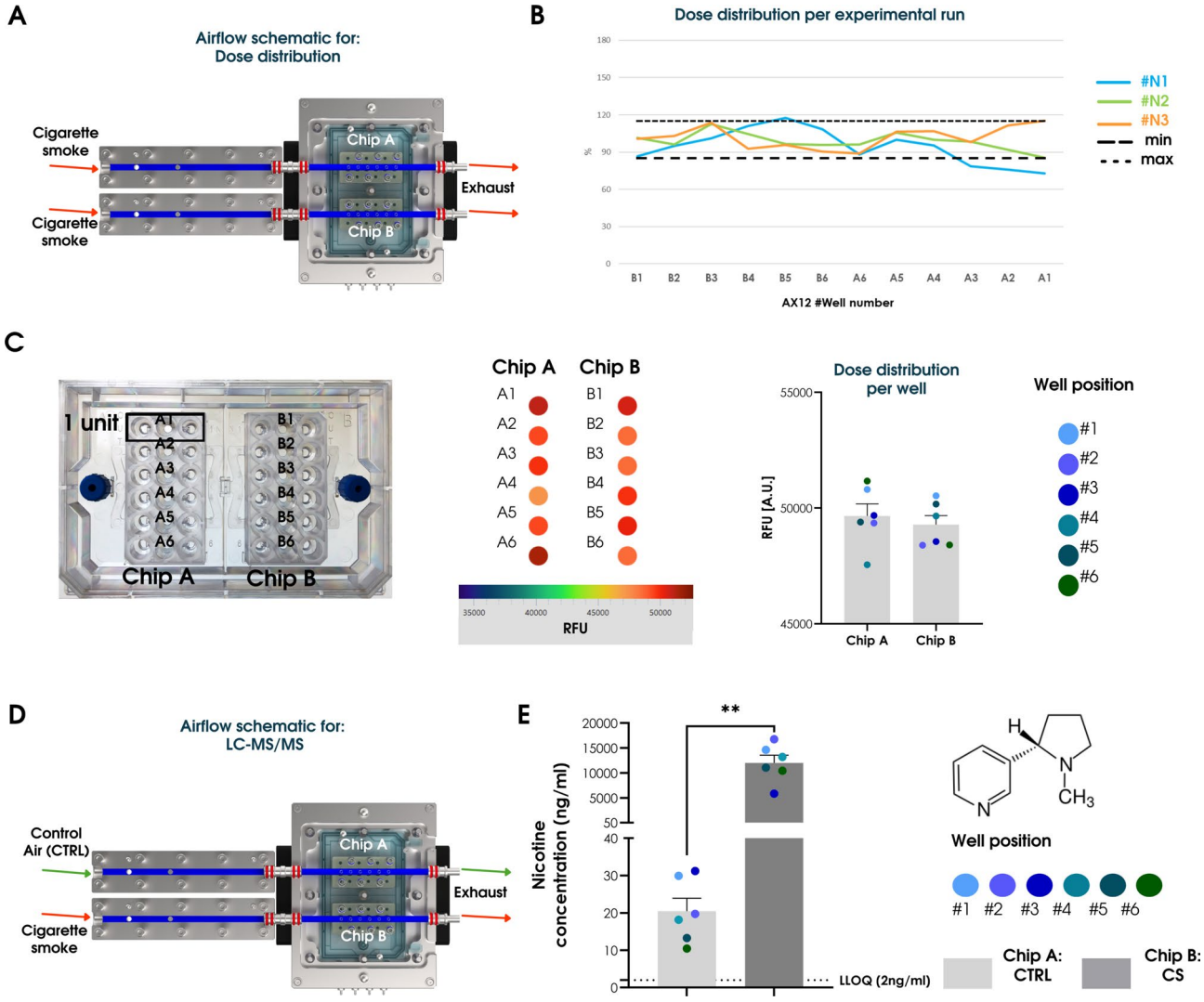

Fig. 3. Dose distribution and exposure analysis using the CFAX12 system (**A**) Diagram illustrating the airflow paths and distribution channels for cigarette smoke in the CFAX12 system. Both Chips (A and B) were exposed to cigarette smoke for this study. (**B**) Consistent dose distribution across multiple experimental runs (N#1, 2, 3). The graph plots indicate the relative dose received by each well (A1–A6 and B1–B6) in the AX12. The dotted lines represent the minimum and maximum acceptable dose range. (**C**) Image of the AX12, highlighting the positioning of Chip A and Chip B containing six individual alveolar units each. Heatmap and bar graph depict the dose distribution across the wells of the AX12 chip based on fluorescence intensity (in RFU—Relative Fluorescence Units). (**D**) Schematic airflow paths for cigarette smoke in Chip B and control air in Chip A in the setup for nicotine distribution study. (**E**) Concentration of nicotine (in ng/ml) within the wells of Chip A and Chip B is depicted. The individual dots represent measurements from specific wells. Lower limit of quantification (LLOQ) for nicotine concentration was at 1 ng/ml. Data are shown as mean ± SEM.

degree of uniformity in smoke exposure within each well. Quantitative dose analysis was performed to provide a more detailed assessment of the distribution revealing that individual data points for each well was clustered closely around the mean values (Fig. 3C). To further validate, we measured the concentration of nicotine, cotinine and 3′-hydroxy-cotinine (OH-cotinine) in the exposed wells using mass spectrometry. Nicotine is known to be the primary addictive component of cigarettes and the first known biomarker to assess smoke exposure[41]. Here, Chip A was exposed to control pure air and Chip B to cigarette smoke (Fig. 3D). The concentration levels of nicotine (~6325 ng/ml), cotinine (~15.6 ng/ml) and OH-cotinine (~1.3 ng/ml) revealed consistent levels and increased measurement with CS exposure (Fig. 3E; Supplementary Fig. 3B).

Effect of cigarette smoke extract (CSE)

First, the impact of traditionally used cigarette smoke extract (CSE) on human alveolar epithelial cells (^{AX}iAECs) cultured under submerged static (Fig. 4A) and dynamic stretch (Fig. 4D) conditions in the AX12 was investigated. CSE was pipetted on the apical side of the alveolar epithelial cells in AX12. 24 h (h) after

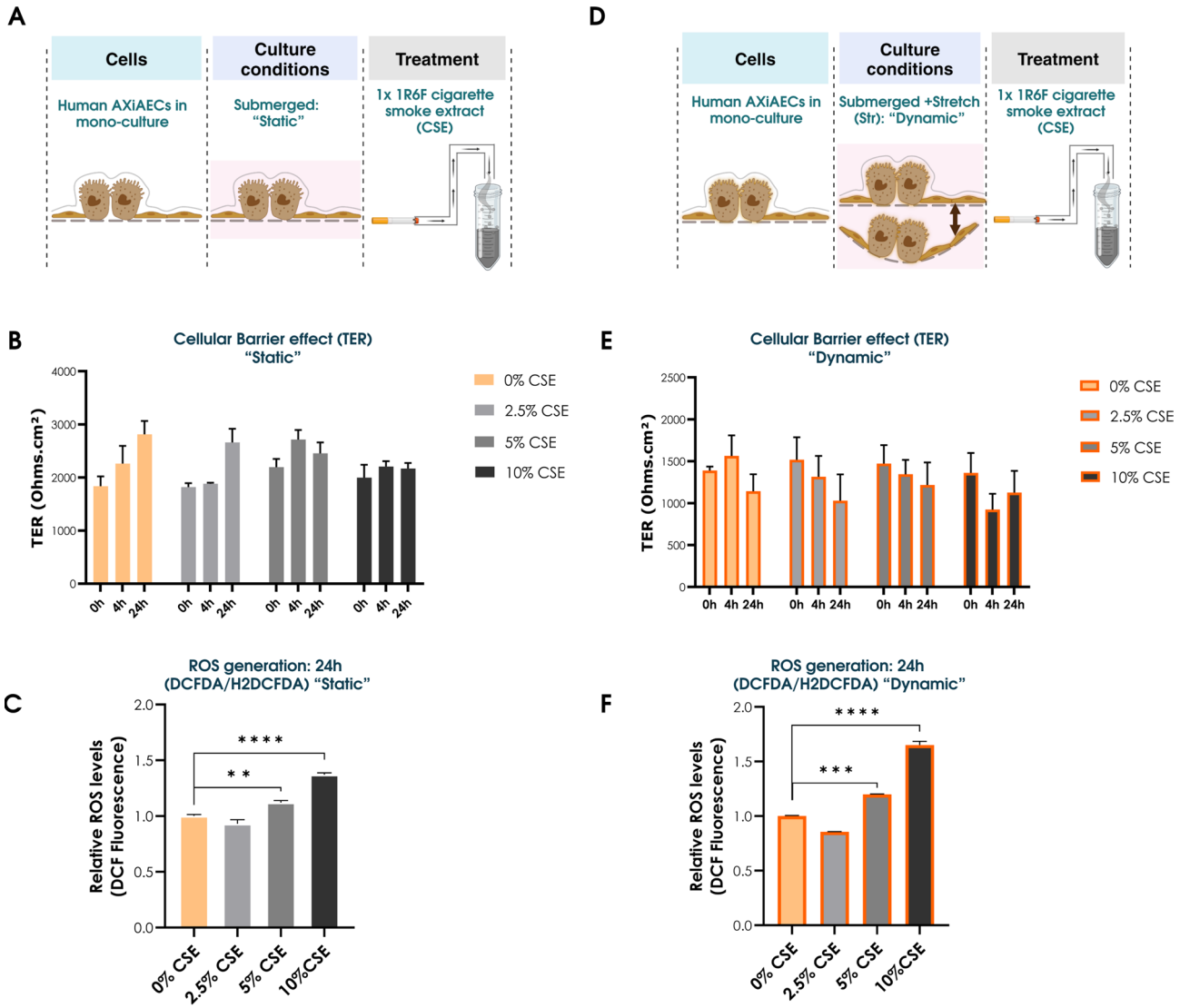

Fig. 4. CSE treatment induced oxidative stress without affecting barrier integrity. (**A**) Overview of cells (^{AX}iAECs), culture conditions (static) and treatment (CSE) performed. (**B**) TER (Ohm cm^2) measured in "static" conditions pre-treatment at 0 h and 4 h and 24 h post-treatment of CSE (0%: Control, 2.5%, 5% and10%) (N = 2; n = 5–6/concentration). (C) ROS generation was measured in the "static" conditions using the DCFDA assay (N = 2; n = 3/concentration). Fluorescence intensity for treated cells were normalized with control (0% CSE) non-treated cells. (D) Overview of cells (^{AX}iAECs) used, culture conditions (dynamic) and treatment (CSE) performed. (E) TER (Ohm.cm^2) measured in "dynamic" conditions pre-treatment at 0 h and 4 h and 24 h post-treatment of CSE (0%: Control, 2.5%, 5% and10%) (N = 2; n = 5–6/concentration). (F) ROS generation was measured in the "dynamic" conditions using the DCFDA assay (N = 2; n = 3/concentration). Fluorescence intensity for treated cells were normalized with control (0% CSE) non-treated cells. Data are shown as mean ± SEM.

instillation, a significant increase in cytotoxicity was observed in the 10%, 25%, 50%, and 100% CSE treated conditions compared to the respective 0% CSE control samples in dynamic conditions only (Supplementary Fig. 4A). This suggest that mechanical forces, in addition to chemical exposure, play a crucial role in modulating cellular responses to cigarette smoke. Due to this heightened cell toxicity and the fewer viable cells remaining at higher concentrated CSE treated samples (starting from 25%), subsequent experiments utilized lower CSE concentrations (0%, 2.5%, 5%, and 10%). TER measurements before treatment (at 0 h) and post-CSE treatment (at 4 h and 24 h) revealed that barrier function was not affected by CSE treatments in both static (Fig. 4B) and dynamic (Fig. 4E) conditions. However, ROS generation significantly increased 24 h post-treatment with 5% and 10% CSE in both static (Fig. 4C) and dynamic (Fig. 4F) conditions, as measured by the DCFDA/H2DCFDA assay. Further, gene expression studies with the dynamic conditions revealed a strong increase in the expression of IL6 and IL8 within the 10% CSE treated samples (Supplementary Fig. 4B). These results indicate that CSE treatment did not significantly impact barrier integrity, but led to increased cytotoxicity, elevated inflammatory markers, and heightened oxidative stress.

Impact of ALI and dynamic culture conditions to CS exposure with the CFAX12

Next, the effects of whole cigarette smoke (CS) exposure were investigated using the CFAX12 system with human alveolar epithelial cells (^{AX}iAECs) cultured under air–liquid interface (ALI) on-chip and tested under static and dynamic (stretch) conditions in the AX12 (Fig. 5A). For this study, one chip was exposed to cigarette smoke and the other chip to control cigarette smoke-free air simultaneously within the same AX12 (schematic Fig. 3D). The integrity of the cellular barrier was evaluated using TER measurements. A significant drop in TER was observed at both 24 h and 48 h post-exposure to CS compared to CTRL samples, indicating a compromised barrier function (Fig. 5B). Cytotoxicity was assessed by measuring LDH release at 24 h and 48 h post-exposure to CS which indicated no substantial effect at either time point compared to the control (CTRL) samples (Fig. 5C). Gene expression levels of TNFα, IL-6, IFNγ, and E-cadherin were measured using qRT-PCR. The results showed no significant changes in the expression of these genes following CS exposure compared to CTRL samples (Supplementary Fig. 5A). Cigarette smoke exposure is known to increase oxidative stress by raising superoxide radicals and reducing intracellular glutathione[42]. Interestingly, ROS levels assessed 48 h post-exposure to CS using the DCFDA/H2DCFDA assay displayed a significant increase in the CS-exposed cells compared to CTRL samples (Fig. 5D). These results collectively demonstrate that while CS exposure under ALI static conditions did not significantly affect cytotoxicity or gene expression of key markers, however it significantly compromised barrier integrity and increased oxidative stress in the alveolar epithelial cells.

To understand how cigarette smoke exposure affects the lung alveolar barrier under breathing-like movements, ^{AX}iAECs were cultured under ALI + Stretch (ALI + Str) conditions (Fig. 5E). One chip was exposed to cigarette smoke, while the other was exposed to control pure air simultaneously within the same AX12 plate, as shown in the schematic (Fig. 3D). The cellular barrier integrity, evaluated using TER measurements, showed a substantial decrease as early as 4 h after CS exposure, which remained consistently decreased until the 48 h endpoint, indicating compromised barrier function (Fig. 5F) in comparison to the healthy non-CS exposed cell barrier (Supplementary Fig. 3A) displaying tight barrier cell junctions. Furthermore, LDH measurements at 24 h and 48 h post-exposure to CS indicated a significantly increased cytotoxic effect at the 48 h time-point compared to the respective CTRL samples (Fig. 5G). Although inflammatory genes such as TNFα, IL-6, and IFNγ did not show drastic changes compared to control, E-cadherin (ECAD) expression significantly decreased within the CS-exposed ALI + Str samples (Supplementary Fig. 5B). Additionally, ROS levels assessed 48 h post-exposure to CS using the DCFDA/H2DCFDA assay displayed a significant increase in the CS-exposed cells compared to CTRL samples (Fig. 5H). These results collectively demonstrate that CS exposure under ALI dynamic conditions elicited more sensitive responses, showing early barrier disruption, increased cytotoxicity, and heightened ROS levels compared to non-stretched static conditions.

Investigating co-culture effects on CS-induced responses using the CFAX12

Building on previous findings that dynamic (stretch) conditions were more sensitive to CS exposure, we investigated dual and triple co-culture models to better understand the impact of CS in complex bio-models in the AX12. The experimental setup is depicted (Fig. 6A), showing a Dual Culture (DC) with alveolar ^{AX}iAECs seeded on the apical side and hLMVEC endothelial cells on the basal side of the membrane. The Triple Culture (TC) models included activated primary blood-derived macrophages (TC pBDMs) or activated human THP1 macrophages (TC THP1) on the apical side along with the alveolar epithelial cells, all maintained under ALI + Str conditions (Fig. 6B) and hLMVEC endothelial cells on the basal side of the membrane. TER measurements indicated a significant drop in barrier integrity at 48 h post CS exposure in the DC model compared to CTRL samples (Fig. 6C). This was also evidenced from the immunofluorescent staining of CS exposed wells displaying reduced tight junctions in apical alveolar epithelial cells (stained with ZO-1) and lower CD31/PECAM-1 gene and protein expression on the basal endothelial cells (Supplementary Fig. 3B, 7E). From the flow cytometry analysis, it was observed that pBDMCs isolated from two donor buffy coats (#D2 and #D3) exhibited a higher percentage of viable cells, exceeding 70% (Supplementary Fig. 2B, C). Consequently, these donor cells were utilized in our subsequent study. Upon activation with M-CSF (Supplementary Fig. 2D), the pBDMCs differentiated into pBDMs, staining positively for CD68 pan-macrophage marker (Supplementary Fig. 2E). In both the TC pBDMs and TC THP1 AX12 models, early barrier disruption was observed starting at 24 h post-exposure and consistent until 48 h time-point, indicating compromised barrier function following CS exposure (Fig. 6C). IL-8 concentration levels, assessed using ELISA, revealed a significant increase in IL-8 secretion in both TC pBDMs and TC THP1 models at the 48 h time-point after CS exposure (Fig. 6D). LDH release measurements showed a significant increase in cytotoxicity in all co-culture models at 48 h post CS exposure (Fig. 6E), suggesting heightened cell death under these complex co-culture conditions. Additionally, PPARγ

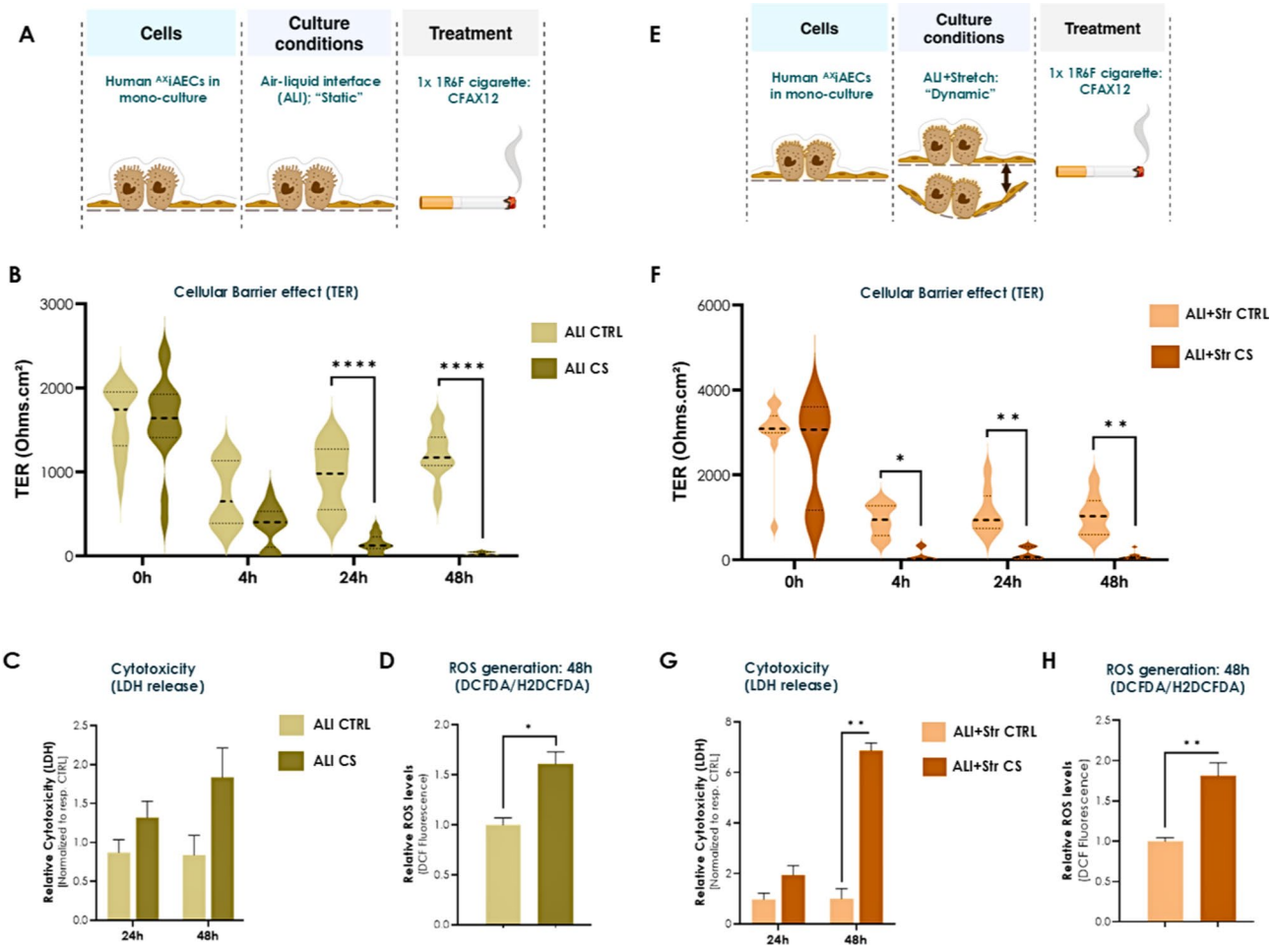

Fig. 5. CS exposure under ALI dynamic conditions induce early barrier disruption and increased cytotoxicity than ALI static. (**A**) Overview of cells (^{AX}iAECs), culture conditions (static) and treatment (CS exposure) performed. (**B**) TER (Ohm cm^2) measured in "ALI, static" conditions pre-exposure at 0 h and 4 h, 24 h and 48 h post-exposure to CS (N = 3; n = 14–16/time-point). Data are shown as violin plots, medians are indicated by black dotted lines. (**C**) Cytotoxicity was calculated from LDH release at 24 h and 48 h after CS exposure (N = 3; n = 6/time-point). (**D**) ROS generation was measured in the "static" conditions using the DCFDA assay (N = 2; n = 4). Fluorescence intensity for treated cells were normalized with control (CTRL) pure air exposed cells. (**E**) Overview of cells (^{AX}iAECs), culture conditions (dynamic; ALI + Str) and treatment (CS exposure) performed. **(F)** TER (Ohm cm^2) measured in "ALI + Str" conditions pre-exposure at 0 h and 4 h, 24 h and 48 h post-exposure to CS (N = 3; n = 14–16/time-point). Data are shown as violin plots, medians are indicated by black dotted lines. (**G**) Cytotoxicity was calculated from LDH release at 24 h and 48 h after CS exposure (N = 3; n = 6/time-point). (**H**) ROS generation was measured in the "ALI + Str" conditions using the DCFDA assay (N = 2; n = 4). Fluorescence intensity for treated cells were normalized with control (CTRL) pure air exposed cells.

expression was decreased in DC and significantly upregulated in TC THP1 model upon CS exposure, suggesting an adaptive response to lipid dysregulation (Supplementary Fig. 7A). Apart from alterations in lipid metabolism, EMT is also well-known hallmark of cigarette-smoke induced COPD[43]. We observed that a decrease in the epithelial marker cadherin 1 (CDH1) (Supplementary 5A,B) and a significant increase in mesenchymal markers like α smooth muscle actin (ACTA2) and Vimentin, particularly in the TC THP1 model, indicating enhanced EMT in response to CS exposure (Supplementary Fig. 7B). ROS levels assessed 24 h post-exposure to CS using the DCFDA/H2DCFDA assay displayed a strong increase in the TC THP1 CS-exposed cells compared to DC CS exposed samples (Supplementary Fig. 7C). Baseline LDH levels were assessed in healthy controls, comparing DC and TC models, as well as ALI and ALI + Str conditions, and no significant differences were observed. Additionally, maximal LDH release (positive control) was evaluated between DC and TC models, showing no significant variation (Supplementary Fig. 7D). These findings indicate that neither increased model complexity (inclusion of macrophages) nor mechanical stretch adversely affected cell viability in the system. In summary, the presence of macrophages in the TC models resulted in an earlier and more pronounced inflammation, lipid alteration and EMT response to CS exposure, highlighting the critical role of these cell types in mediating the cellular response to CS exposure.

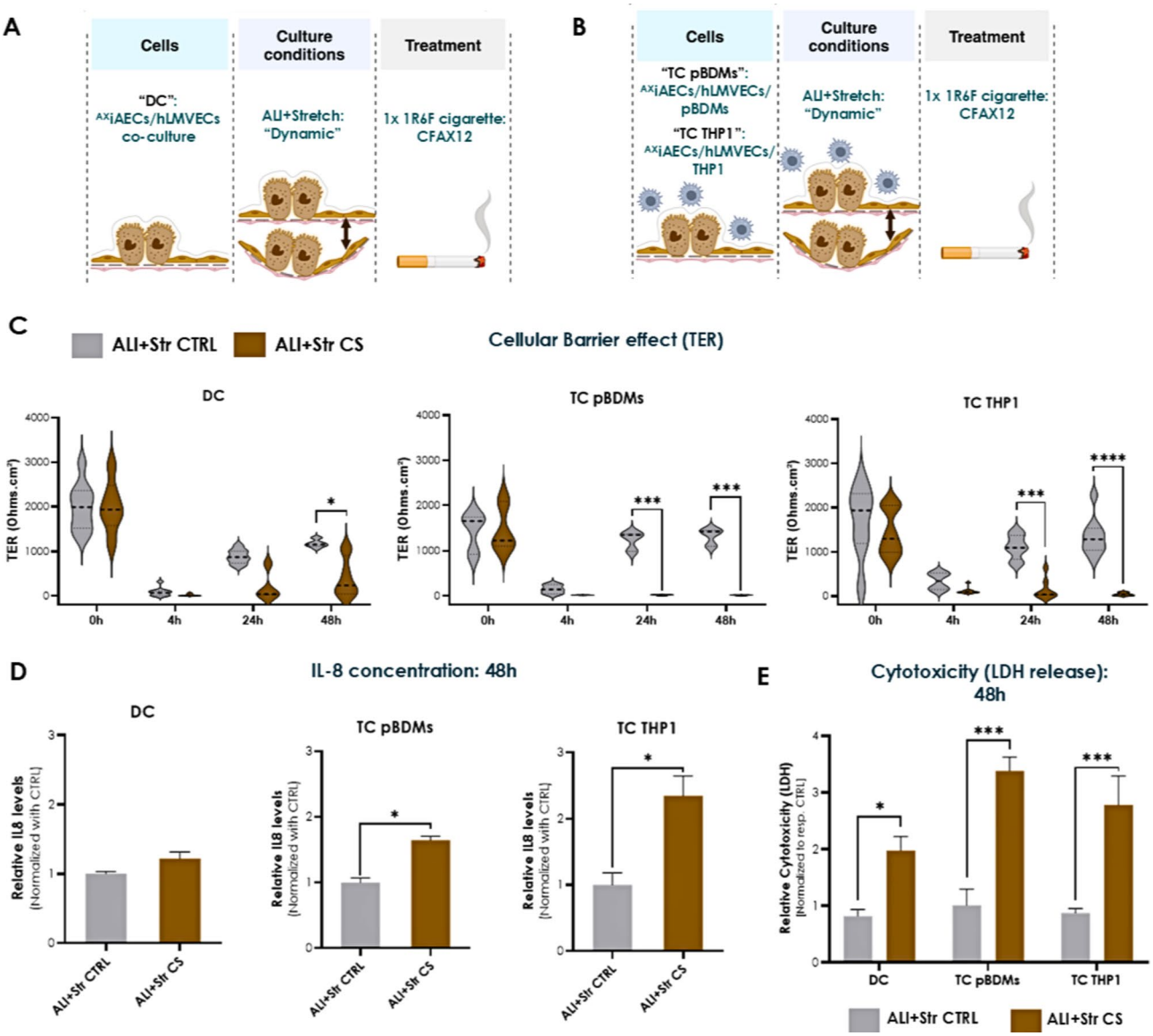

Fig. 6. Differential effects of CS exposure on various co-culture dynamic models. (**A**) Overview of cells used in the dual culture "DC" (^{AX}iAECs/hLMVECs), culture conditions (dynamic; ALI + Str) and treatment (CS exposure) performed. (**B**) Overview of cells used in the triple culture "TC pBDMs" (^{AX}iAECs/hLMVECs/pBDMs) and "TC THP1" (^{AX}iAECs/hLMVECs/THP1), culture conditions (dynamic; ALI + Str) and treatment (CS exposure) performed. (**C**) TER (Ohm cm^2) measured in "ALI + Str" conditions pre-exposure at 0 h and 4 h, 24 h and 48 h post-exposure to CS in DC (N = 3; n = 3/time-point), in TC pBDMs (N = 2; n = 3/time-point) and TC THP1 (N = 3; n = 3/time-point). Data are shown as violin plots, medians are indicated by black dotted lines. (**D**) The levels of IL-8 (pg/ml) in the supernatants collected from the cells were measured by ELISA in all the co-culture models. (**E**) Cytotoxicity was calculated from LDH release at 48 h time-point after CS exposure (N = 2; n = 3/time-point for all models). Data are shown as mean ± SEM.

Influence of interfacial pulmonary surfactant layers on CS exposure with the CFAX12

In the final study, the TC THP1 co-culture model was utilized and pre-treated with surfactant to assess the outcome of CS exposure in the presence of a surfactant layer formed at the air-exposed interface, using the CFAX12 (Fig. 7A). The surfactant preparation used was Curosurf, a clinical formulation of porcine origin widely used in the treatment of preterm neonates. This surfactant contains most of surfactant lipids plus the hydrophobic proteins SP-B and SP-C, which are responsible for the spreading of the lipid/protein complexes to form layers at the air-exposed surface of the alveolar epithelium. The extreme hydrophobicity of these proteins makes Curosurf very low immunogenic in a humanized context. Due to low cell isolation count and donor variability with the primary macrophages (pBDMs), the well-characterized THP1 macrophages were used for this part of the study. Although the presence of surfactant could not recover the barrier loss due to the CS exposure induced stress (Supplementary Fig. 5C), immunofluorescent staining revealed substantially less barrier breakdown along with higher nuclei count (more visible number of viable cells) in the presence of surfactant in comparison to

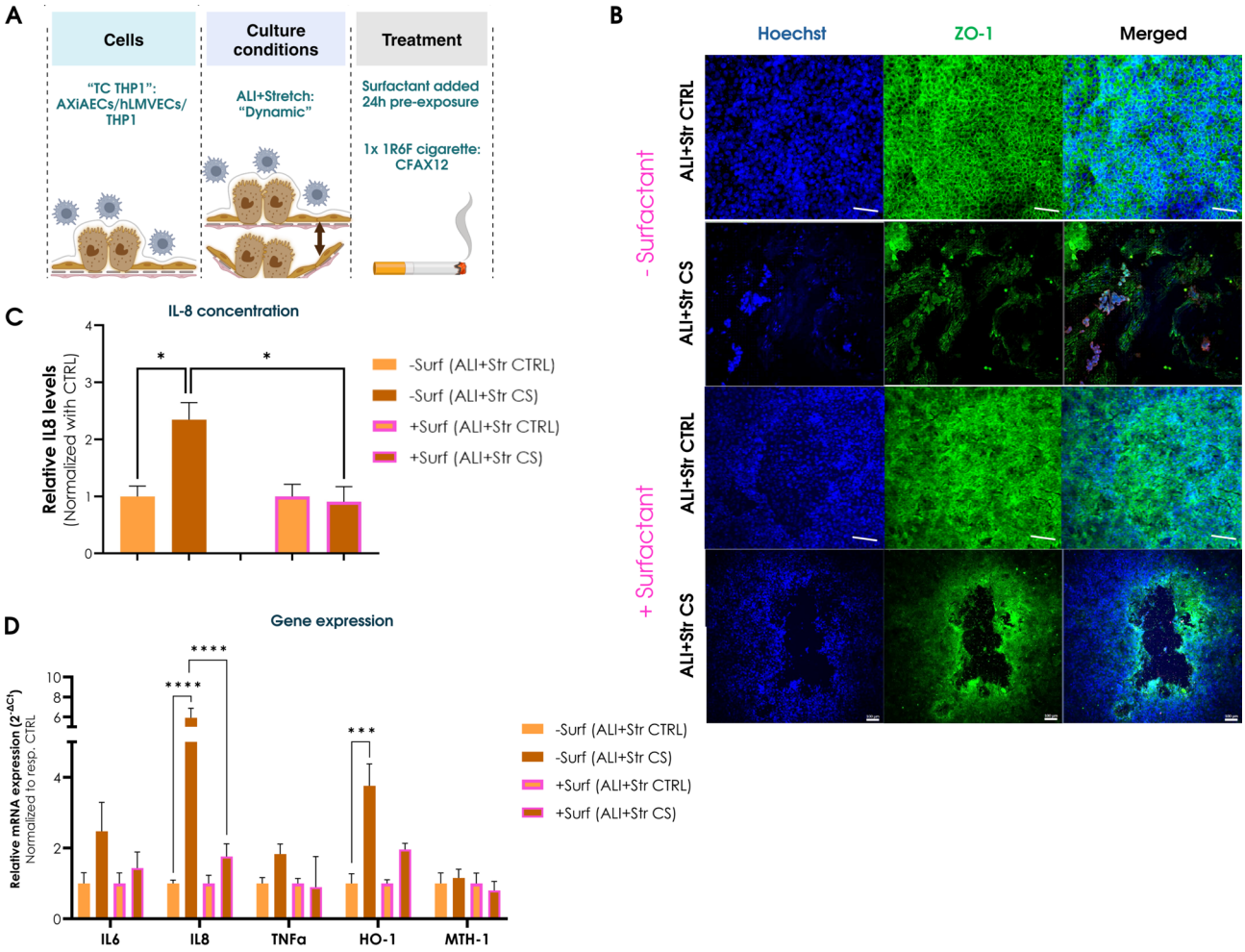

Fig. 7. Apical surfactant addition demonstrates potential protective effects against CS exposure. (**A**) Overview of cells used in the triple culture "TC THP1" (AXiAECs/hLMVECs/THP1), culture conditions (dynamic; ALI + Str) and treatment (Surfactant pre-treated followed by CS exposure) performed. (**B**) Representative immunofluorescence staining of CTRL ALI + Str (− Surfactant) cells (top row; scale bar 50 µm), CS exposed ALI + Str (-Surfactant) cells (second row; scale bar 50 µm), CTRL ALI + Str (+ Surfactant) cells (third row; scale bar 100 µm), CS exposed ALI + Str (+ Surfactant) cells (fourth row; scale bar 100 µm). Cells were stained for Zonula Occludens 1 (ZO-1, in green) and nuclei (Hoechst, in blue). (**C**) IL-8 concentration (pg/ml) measured from apical supernatants collected from the CTRL and CS exposed wells pre-treated with and without surfactant (+ Surf or -Surf) via ELISA assay (N = 2; n = 6/condition). (**D**) mRNA was harvested at 48 h time-point with and without surfactant (+ Surf or -Surf) post-exposure to CS. qRT-PCR study for inflammation (Interleukin 6, IL6; Interleukin 8, IL8; Tumor Necrosis Factor α, TNFα) and oxidative stress-related (Heme Oxygenase 1, HO-1; Human MutT Homolog 1, MTH-1) genes were conducted in all -Surf and + Surf CS exposed and CTRL samples (N = 2, n = 3). Data are shown as mean ± SEM.

the non-surfactant treated cells after CS exposure under ALI + Str conditions (Fig. 7B). Additionally, under ALI + Str conditions, surfactant exposed cells were associated with significantly lower levels of IL8 secretion at the supernatants (Fig. 7C), as well as decreased IL8 gene expression (Fig. 7D) after CS exposure in comparison to the non-surfactant treated CS exposed samples. On the other hand, the cytotoxic effects appeared to be slightly reduced with the addition of surfactant under dynamic conditions (Supplementary Fig. 6C) suggesting a potential protective effect of surfactant on cells exposed to CS.

Discussion

Chronic respiratory diseases such as COPD and lung cancer are leading causes of morbidity and mortality globally, with CS being a primary risk factor[3]. Conventional in vitro models frequently fall short in replicating the intricate lung microenvironment and the dynamic exposure conditions present in vivo, thereby reducing their predictive accuracy in preclinical studies[26,44]. Advanced models like the CFAX12 integrated with a lung-on-chip technology are crucial for bridging this gap, providing a more physiologically relevant platform to study CS-induced lung damage. This innovative approach allows for the simultaneous exposure of human relevant

cell types to whole smoke in a controlled environment, closely mimicking the actual conditions experienced by human lung tissue.

The CFAX12 platform presented in this study offers significant advantages over traditional models that typically utilize cigarette smoke extract (CSE) treatment and culture cells under submerged conditions, which do not accurately represent the ALI conditions found in the human lung[45,46]. Additionally, it is well-documented that CSE elicits distinct cellular and molecular effects compared to CS in animal models[17]. This distinction is evident also in our studies, where CSE impacts cytotoxicity and ROS generation without significantly affecting cell barrier integrity or inflammatory genes (Fig. 4, Supplementary Fig. 4). Furthermore, preparation of CSE includes various protocols established in different labs which leads to inter-lab variations in the composition of CSE leading to differential effect of these extract used in downstream studies. Moreover, the in vitro models used for CSE treatments often lack the mechanical forces that are crucial for mimicking the respiratory movements in vivo. The CFAX12 system, however, incorporates ALI and breathing-like motions (stretch; Str) conditions, providing a more realistic simulation of the lung environment which is crucial for distal lung cell function[26].

Next, we demonstrated that replicating key aspects of the lung alveolar micro-environment specifically, the air–liquid interface (ALI), breathing-like motions (stretch), and the inclusion of an immune component significantly enhances the sensitivity of the smoke-induced lung-on-chip model. This comprehensive approach not only improves the physiological relevance of the model but also reveals synergistic effects that are not detectable when these factors are absent. Our results demonstrated that under combined ALI and Str conditions, CS exposure led to a significant and early drop in TER, cytotoxicity and reduced expression of cell–cell adhesion gene (Cadherin 1; CDH1) expression indicating compromised barrier integrity along with heightened cytotoxicity (Fig. 5F, G; Supplementary Fig. 5B). In contrast, static ALI conditions showed a late decrease in TER and less pronounced cytotoxicity, emphasizing the importance of mechanical forces in exacerbating the effects of CS on the epithelial barrier (Fig. 5B, C; Supplementary Fig. 5A). Interestingly, our previous studies observed a similar significant impact of breathing-like stretch on the uptake of inhaled substances by the alveolar barrier[26]. Cyclic mechanical stretch plays a crucial role in modulating lung responses to cigarette smoke exposure, as lung cells experience continuous biomechanical forces during breathing. Mondoñedo et al.[47] demonstrated that when lung tissue is subjected to cyclic stretch during CSE treatment, there is a significant increase in inflammatory cytokine IL-1β and proteolytic enzymes such as MMP-1, which are key contributors to emphysema progression. Moreover, stretch influences oxidative stress responses and tissue remodeling, as regions of the lung exposed to abnormal mechanical forces become more susceptible to cigarette smoke-induced injury. This aligns with findings showing that mechano-transduction pathways regulate epithelial integrity and inflammatory cascades in COPD pathogenesis. Moreover, nicotine has been shown to down-regulate both the proliferation rate and biosynthesis of glycan molecules[48], important components of the ECM. Hence, CS exposure may additionally initiate abnormal ECM remodeling process, a well-established hallmark of COPD[49–51]. In this context, future studies would benefit from utilizing a biological relevant, biodegradable membrane-integrated lung-on-chip model[52] to better assess smoke-induced ECM remodeling. These observations highlight the importance of incorporating dynamic and biophysical conditions in COPD research to better understand the complex interactions between cell types and mechanical forces in the lung.

Nicotine is known to rapidly metabolize into cotinine and OH-Cotinine, indirectly contributing to more heightened ROS accumulation[53,54]. In humans, it has a very short half-life and is rapidly metabolized by liver enzyme CYP2A6 into cotinine and OH-Cotinine, which in turn can be utilized as clinical biomarkers to assess smoking-status[55]. In our LC–MS/MS studies, smoke trapped in PBS was collected immediately after exposure from the CFAX12. In this setting, CYP2A6 metabolism and conversion of nicotine to its metabolites is unlikely and consequently high metabolite concentrations, typically reported in humans, were not observed. The observed rise in cotinine concentration (~0.2% of nicotine measured concentration) in the PBS can be explained by its presence in the tobacco leaves[56], whilst there is no direct explanation for the observed OH-cotinine in the PBS (~0.02% of nicotine concentration) (Supplementary Fig. 3B). The nicotine concentration measurements confirmed the system's ability to deliver consistent smoke exposure across all the wells in the AX12 plate (Fig. 3E), validating its robustness and accuracy. This enhanced physiological relevance translates to more reliable and translatable data for preclinical research. Furthermore, the nicotine concentration level (~6.5–7 µg/ml) obtained per well in our studies related with previous smoke exposure reports utilizing the 1R6F cigarettes[57,58], although future in-depth studies are required to standardize the in vitro to in vivo smoker dose correlation to better assess human smoking responsiveness. In our current modeling approach, the chronic exposure regimen led to excessive cytotoxicity, limiting our ability to assess long-term endpoints and subtle inflammatory responses. Therefore, we standardized our experiments using acute dosing (single cigarette), which allowed us to capture early cellular responses while preventing overt toxicity. Moving forward, it will be essential to optimize the exposure conditions to support a chronic smoke regimen, including adjustments to higher dilution flow rates and longer exposure duration, to enable a more controlled and physiologically relevant modeling of chronic smoke-induced effects. Further refinements of the cell model and exposure system will be critical in ensuring long-term cell viability while maintaining sensitivity to pathophysiological changes over extended exposure periods.

In addition, the inclusion of macrophages in the TC models (TC pBDMs or TC THP1) demonstrated an early and more pronounced response to CS exposure compared to DC (epithelial/endothelial) models. This was evident from the significant drop in TER, increased IL-8 secretion along with enhanced cytotoxic reactiveness in TC culture models compared to the DC culture model (Fig. 6), suggesting that macrophages play a critical role in mediating inflammatory responses to CS. Single-cell RNA sequencing studies in murine smoke models have identified an excessive influx of monocyte-derived macrophage subset population responsible for heightened inflammation and ECM remodeling, a finding that has also been validated in emphysematous COPD patients[59]. The initial dip in TER observed in all control (CTRL) samples around 4 h post-exposure, followed by recovery,

suggests that the cells may be sensitive to the exposure conditions, including the impact of cigarette smoke-free control air, and due to being kept outside the incubators. However, the subsequent increase in TER indicates that the CTRL cells adapt and recover, reestablishing a tight barrier (Figs. 5B, F, 6C). Additionally, it is known that primary alveolar macrophages have a higher potential to incite inflammatory responses compared to blood-derived macrophages. However, obtaining and culturing human primary alveolar macrophages is challenging due to their deep location within the lung and their terminal differentiation status, which was out of scope for this study. Therefore, subsequent studies should examine the influence of including primary lung alveolar macrophage in such smoke-induced studies in vitro. Within the TC THP1 cell model, the presence of macrophages amplified ROS generation, as evidenced by a 7.4-fold increase in DCFDA levels, compared to 5.2-fold in DC culture conditions upon CS exposure (Supplementary Fig. 7C). Additionally, key oxidative stress-associated genes, including HO-1, Catalase, and SOD1, were significantly upregulated in the TC THP1 CS model relative to the DC model (Fig. 7D, Supplementary Fig. 6D). Given that ROS generation is highly time-sensitive, it is possible that earlier timepoints in the DC model would yield more sensitive readouts of oxidative stress dynamics. This suggests that incorporating earlier sampling intervals may be necessary to fully capture the kinetics of ROS induction and improve the resolution of early-stage smoke-induced oxidative damage. In addition, phagocytosis is also an essential process for clearing apoptotic cells and maintaining lung homeostasis, but CS impairs this process in COPD, leading to persistent inflammation[60]. Studies show that smoke exposure reduces macrophage phagocytic ability by downregulating key recognition receptors and MFG-E8, a crucial bridging molecule for apoptotic cell clearance[61]. This results in the accumulation of apoptotic cells, triggering secondary necrosis and further lung damage. While phagocytosis was beyond the scope of our study, its role in COPD progression highlights the need for future research to better understand alterations in macrophage functions also including polarization and formation of foamy macrophages.

Our findings reveal a decreased PPARγ expression in dual-culture conditions (without macrophages) and a significant upregulation in triple-culture conditions (with macrophages) upon cigarette smoke exposure (Supplementary Fig. 7A), suggesting a macrophage-dependent regulation of PPARγ. This aligns with previous studies indicating that PPARγ is highly expressed in alveolar macrophages and plays a pivotal role in modulating inflammation and oxidative stress responses[62,63]. Macrophage presence may contribute to increased PPARγ expression via TLR4-mediated signaling, as cigarette smoke is known to induce PPARγ upregulation through inflammatory pathways in alveolar macrophages[64]. Additionally, PPARγ is a key regulator of lipid metabolism and surfactant homeostasis, both of which are known to be disrupted in COPD. CS exposure is known to alter lipid metabolism by impairing PPARγ signaling, leading to increased lipid accumulation in alveolar macrophages, which exacerbate chronic inflammation[65]. The upregulation of PPARγ in the presence of macrophages might thus reflect a compensatory mechanism aimed at enhancing lipid catabolism and mitigating smoke-induced lipid dysregulation, oxidative stress and inflammation.

The presence of layers of pulmonary surfactant at the apical side demonstrated in our studies a potential protective effect against CS exposure. Although TER and cytotoxicity did not fully recover post-CS exposure, inflammation markers such as IL8 cytokine secretion and IL8 and HO-1 gene levels were significantly reduced, suggesting that surfactant helps mitigate some of the inflammatory damage caused by CS (Fig. 7C, D; Supplementary Fig. 5C, E). Under static ALI conditions, the presence of surfactant resulted in minor but not significant improvements in IL8 secretion (Supplementary Fig. 5D), further emphasizing the enhanced sensitivity of dynamic models to smoke exposure. Compression-expansion breathing-like dynamics relates to the formation of complex surfactant structures at the air–liquid interface, which may in part enhance the somehow protective barrier effect against airborne chemicals. CS and its component, acrolein, have been identified to induce modifications in the function of surfactant proteins SP-A, SP-B, and SP-C while significantly lowering SP-D levels[66–68]. Another school of thought suggests possible chemical alterations of the surfactant phospholipid composition and structure due to interactions with gaseous components from cigarette smoke[69,70]. Exposure to CS may therefore have an additional impact on pulmonary surfactant structure and function, including its ability to maintain the presence of a protective coating layer at the epithelial surface. This extreme situation has not been analyzed here as it is far from the scope of this work but guarantees future studies in an alveolar-mimicking scenario such as the one recreated in our models. Moreover, the presence and role of surfactant as a protective physical barrier preventing damage to underlying cells is also well-documented[71–74]. It is well established that surfactant lipids and proteins down-regulate inflammation through direct molecular interactions with both epithelial and immune cells. It is also conceivable that the lipid-rich surfactant layer act as scavenger of hydrophobic components of CS, captured from the air phase, and somehow retained from the exposure to the epithelial lining. Some of the surfactant components, such as unsaturated and alkyl phospholipids, have been proposed to act as antioxidants, therefore reducing the exposure of cell membranes to ROS. A study has shown that pulmonary surfactant reduces oxidative stress and mitigates inflammation from inhaled toxicants. It can decrease lipid peroxidation and restore antioxidant enzyme activity (e.g., catalase, superoxide dismutase), which are otherwise impaired by CS. Additionally, surfactant phospholipids and proteins (SP-A, SP-D) modulate immune responses by interacting with macrophages, reducing excessive pro-inflammatory cytokine release[75]. Moreover, surfactant inclusion has been reported to lower ROS levels and protect mitochondrial function by preserving ATP production in lung alveolar cells[76], which aligns with our findings where its presence significantly reduced IL-8 gene expression and oxidative stress markers following CS exposure. These mechanisms suggest a potential barrier-protective and immunomodulatory role of surfactant in our CFAX12 model. However, which of these and other potential mechanisms are responsible for the protective effects shown here by surfactant against CS need further studies. The limitations of the current research, such as the investigation of the incomplete recovery of TER in the presence of surfactant in samples post-CS exposure, also needs to be addressed in future research targeting the need of additional components and contributions to fully protect barrier integrity. Exploring different concentrations and combinations of surfactants, including

human native surfactant[72] containing the highly immunomodulatory surfactant collectins SP-A and SP-D, along with other protective agents such as anti-inflammatory drugs or antioxidants, could yield more effective strategies for mitigating smoke-induced damage.

Pulmonary hypertension is known to be clinically associated with COPD and studies have established vascular remodeling and aberrant activation and function of the endothelial cells in CS-induced emphysema[77]. Hence from this growing evidence, it might be beneficial to look more closely into the endothelial activation and develop strategies to inhibit or repair this abnormal response as a measure to combat CS-induced associated cardiovascular and other health effects. Interestingly, as our results indicated an ongoing EMT following CS exposure, evidenced by decreased epithelial marker CDH1 and increased mesenchymal markers ACTA2 and Vimentin (Supplementary Fig. 7B, 5A, B). Including fibroblasts or other mesenchymal cell populations in co-culture models could be crucial for studying smoke-induced effects, as these cells contribute to extracellular matrix remodeling, fibrosis, and epithelial-mesenchymal interactions, which are key processes in COPD and emphysema progression. Additionally, their presence modulates epithelial responses to cigarette smoke by influencing cytokine signaling, oxidative stress adaptation, and tissue repair mechanisms, providing a more physiologically relevant model for inhalation toxicity studies[78–80]. This could provide insights into the interactions between different cell types and how they contribute to cigarette smoke-induced damage and repair processes.

Additionally, the CFAX12 system can be adapted to investigate other respiratory diseases and toxic exposures, such as the effects of e-cigarette vapor or heated tobacco products on human lung health. This adaptation could facilitate crucial studies comparing the toxicity and safety profiles of new-generation tobacco products with traditional combustion cigarettes. For instance, the system could be used to quantify oxidative stress, inflammatory cytokine release, and epithelial barrier integrity changes following exposure to different e-cigarette exposure, providing a comparative framework for regulatory assessments. Furthermore, CFAX12 could elucidate the progression and pathomechanism of vaping-associated pulmonary injury (EVALI), identifying key associated molecular signatures. Finally, integrating advanced imaging techniques and high-throughput omics approaches, such as single-cell transcriptomics, spatial proteomics, and metabolomics, could provide deeper insights into the molecular and cellular responses to cigarette smoke and other new alternative tobacco products. This comprehensive approach would enable the identification of novel biomarkers and therapeutic targets, advancing our understanding of smoke-induced health effects, while paving the way for more personalized and effective treatments.

Conclusion

The CFAX12 system uniquely integrates a whole smoke exposure platform with a breathing lung-on-chip technology, providing a physiologically relevant method for studying cigarette smoke-induced changes at the cellular level. Unlike conventional in vitro systems, the CFAX12 better mimics the in-vivo smoke inhalation situation, with the alveolar epithelial cells cultured at ALI, being directly exposed to the smoke rather than cigarette smoke extract (CSE) in liquid form. In addition, the dynamic environment of the air-blood barrier makes the cells more sensitive and the barrier more responsive to CS-induced changes. This is critical, as our study demonstrates that mechanical stretch significantly intensifies smoke-induced damage, with notable differences observed in barrier integrity, oxidative stress, and inflammatory responses under dynamic ALI conditions compared to static ALI conditions. Additionally, the presence of macrophages in triple-culture models further amplified the inflammatory response, highlighting the crucial role of immune cells in mediating lung injury scenarios. This model also addresses the limitations of traditional cigarette smoke extract (CSE) studies, which do not fully capture the complex chemical milieu and mechanical forces present during actual smoke inhalation. Our results clearly show that whole smoke exposure leads to differential effects of cellular damage and inflammation compared to CSE, emphasizing the necessity of using whole smoke for realistic toxicity assessments. The CFAX12 platform, therefore, proves to be an essential tool for preclinical research, enabling detailed exploration of the cellular and molecular mechanisms underlying cigarette smoke-related diseases and facilitating the development of targeted therapeutic strategies. Its ability to simulate majority of the spectrum for smoke exposure conditions and its incorporation of mechanical forces make it a reliable model for advancing our understanding of respiratory diseases and improving the translation of preclinical findings to clinical applications.

Data availability

All data generated or analyzed during this study are included in this published article [and its supplementary information files]. Preliminary study datasets analyzed for this study are available from the corresponding author on reasonable request.

Received: 7 August 2024; Accepted: 28 April 2025
Published online: 25 May 2025

References

1. Chen, S. et al. The global economic burden of chronic obstructive pulmonary disease for 204 countries and territories in 2020–50: A health-augmented macroeconomic modelling study. *Lancet Glob. Health* **11**(8), e1183–e1193 (2023).
2. WHO. Smoking is the leading cause of chronic obstructive pulmonary disease (2023). https://www.who.int/news/item/15-11-2023-smoking-is-the-leading-cause-of-chronic-obstructive-pulmonary-disease
3. Parris, B. A., O'Farrell, H. E., Fong, K. M. & Yang, I. A. Chronic obstructive pulmonary disease (COPD) and lung cancer: Common pathways for pathogenesis. *J. Thorac. Dis.* **11**(Suppl 17), S2155–S2172 (2019).
4. Bezerra, F. S. et al. Oxidative stress and inflammation in acute and chronic lung injuries. *Antioxidants* **12**(3), 548 (2023).

5. Domej, W., Oettl, K. & Renner, W. Oxidative stress and free radicals in COPD-implications and relevance for treatment. *Int. J. COPD* **9**, 1207–1224 (2014).
6. Hou, W. et al. Cigarette smoke induced lung barrier dysfunction, EMT, and tissue remodeling: A possible link between COPD and lung cancer. *BioMed Res. Int.* **2019**, 2025636 (2019).
7. Chen, H. et al. Lipid metabolism in chronic obstructive pulmonary disease. *Int. J. COPD* **14**, 1009–1018 (2019).
8. Gillenwater, L. A. et al. Metabolomic profiling reveals sex specific associations with chronic obstructive pulmonary disease and emphysema. *Metabolites* **11**(3), 161 (2021).
9. Bissonnette, E. Y., Lauzon-Joset, J.-F., Debley, J. S. & Ziegler, S. F. Cross-talk between alveolar macrophages and lung epithelial cells is essential to maintain lung homeostasis. *Front. Immunol.* **11**, 583042 (2020).
10. Bedford, R. et al. A multi-organ, lung-derived inflammatory response following in vitro airway exposure to cigarette smoke and next-generation nicotine delivery products. *Toxicol. Lett.* **387**(387), 35–49 (2023).
11. Lagowala, D. A. et al. Microphysiological models of lung epithelium-alveolar macrophage co-cultures to study chronic lung disease. *Adv. Biol.* **8**, e2300165 (2023).
12. Mortaz, E. & Adcock, I. A. Limitation of COPD studies in animal modeling. *Tanaffos* **11**(3), 7–8 (2012).
13. Serré, J. et al. Enhanced lung inflammatory response in whole-body compared to nose-only cigarette smoke-exposed mice. *Respir. Res.* **22**(1), 86 (2021).
14. Golding, H., Khurana, S. & Zaitseva, M. What is the predictive value of animal models for vaccine efficacy in humans? The importance of bridging studies and species-independent correlates of protection. *Cold Spring Harb. Perspect. Biol.* **10**(4), a028902 (2018).
15. Junhee Seok, H. et al. Genomic responses in mouse models poorly mimic human inflammatory diseases. *Proc. Natl. Acad. Sci. U. S. A.* **110**(9), 3507–3512 (2013).
16. Miller-Holt, J. et al. Use of new approach methodologies (NAMs) to meet regulatory requirements for the assessment of tobacco and other nicotine-containing products. *Front. Toxicol.* **4**, 943358 (2022).
17. Elliott, M., Sisson, J., West, W. & Wyatt, T. Differential in vivo effects of whole cigarette smoke exposure versus cigarette smoke extract on mouse ciliated tracheal epithelium. *Exp. Lung Res.* **32**(3–4), 99–118 (2006).
18. Kim, Y. H. et al. Comparison of volatile organic compounds between cigarette smoke condensate (CSC) and extract (CSE) samples. *Environ. Health Toxicol.* **33**(3), e2018012 (2018).
19. Pryor, W. A. & Stone, K. Oxidants in cigarette smoke radicals, hydrogen peroxide, peroxynitrate, and peroxynitrite. *Ann. N. Y. Acad. Sci.* **686**(1), 12–27 (1993).
20. Smith, C. J. & Hansch, C. The relative toxicity of compounds in mainstream cigarette smoke condensate. *Food Chem. Toxicol.* **38**(7), 637–646 (2000).
21. Agraval, H., Sharma, J. R. & Yadav, U. C. S. Method of preparation of cigarette smoke extract to assess lung cancer-associated changes in airway epithelial cells. *Methods Mol. Biol.* **2413**, 121–132 (2022).
22. Ingber, D. E. Human organs-on-chips for disease modelling, drug development and personalized medicine. *Nat. Rev. Genet.* **23**(8), 467–491 (2022).
23. Baptista, D. et al. 3D lung-on-chip model based on biomimetically microcurved culture membranes. *ACS Biomater. Sci. Eng.* **8**(6), 2684–2699 (2022).
24. Nawroth, J. C. et al. Breathing on chip: Dynamic flow and stretch accelerate mucociliary maturation of airway epithelium in vitro. *Mater. Today Bio.* **21**, 100713 (2023).
25. Marrer-Berger, E. et al. The physiological interactome of TCR-like antibody therapeutics in human tissues. *Nat. Commun.* **15**(1), 3271 (2024).
26. Sengupta, A. et al. A multiplex inhalation platform to model in situ like aerosol delivery in a breathing lung-on-chip. *Front. Pharmacol.* **14**, 1114739 (2023).
27. Singh, A. V. et al. Advances in smoking related in vitro inhalation toxicology: A perspective case of challenges and opportunities from progresses in lung-on-chip technologies. *Chem. Res. Toxicol.* **34**(9), 1984–2002 (2021).
28. Benam, K. H. et al. Matched-comparative modeling of normal and diseased human airway responses using a microengineered breathing lung chip. *Cell Syst.* **3**(5), 456–466 (2016).
29. Benam, K. H., Novak, R., Ferrante, T. C., Choe, Y. & Ingber, D. E. Biomimetic smoking robot for in vitro inhalation exposure compatible with microfluidic organ chips. *Nat. Protoc.* **15**(2), 183–206 (2020).
30. Mathis, C. et al. Human bronchial epithelial cells exposed in vitro to cigarette smoke at the air-liquid interface resemble bronchial epithelium from human smokers. *Am. J. Physiol. Lung Cell. Mol. Physiol.* **304**(7), L489-503 (2013).
31. Thorne, D. et al. Characterization of a Vitrocell® VC 10 in vitro smoke exposure system using dose tools and biological analysis. *Chem. Cent. J.* **7**(1), 146 (2013).
32. Li, Z. et al. Analysis of the response to cigarette smoke exposure in cell coculture and monoculture based on bionic-lung microfluidic chips. *Anal. Chim. Acta* **1300**, 342446 (2024).
33. Li, Z. et al. Combining a lung microfluidic chip exposure model with transcriptomic analysis to evaluate the inflammation in BEAS-2B cells exposed to cigarette smoke. *Anal. Chim. Acta* **1287**, 342049 (2023).
34. Makwana, O. et al. Impact of cigarette versus electronic cigarette aerosol conditioned media on aortic endothelial cells in a microfluidic cardiovascular model. *Sci. Rep.* **11**(1), 4747 (2021).
35. Sengupta, A. et al. A new immortalized human alveolar epithelial cell model to study lung injury and toxicity on a breathing lung-on-chip system. *Front. Toxicol.* **4**, 840606 (2022).
36. Stucki, J. D. et al. Medium throughput breathing human primary cell alveolus-on-chip model. *Sci. Rep.* **8**(1), 14359 (2018).
37. Lipps, C. et al. Expansion of functional personalized cells with specific transgene combinations. *Nat. Commun.* **9**(1), 994 (2018).
38. Kletting, S. et al. Co-culture of human alveolar epithelial (hAELVi) and macrophage (THP-1) cell lines. *Altex* **35**(2), 211–222 (2018).
39. Van Der Velpen, V. et al. A validated single-step saliva and serum sample extraction LC-MS/MS method for the analysis of nicotine, cotinine and 3'-hydroxycotinine for clinical vaping studies. *J. Pharm. Biomed. Anal.* **15**(28), 116703 (2025).
40. Li, Y. et al. Fluorescent property of carbon dots extracted from cigarette smoke and the application in bio-imaging. *Opt. Express* **30**(26), 47026–47037 (2022).
41. Schick, S. F. et al. Biomarkers of exposure to new and emerging tobacco delivery products. *Am. J. Physiol. Lung Cell. Mol. Physiol.* **313**(3), L425–L452 (2017).
42. Seo, Y. S., Park, J. M., Kim, J. H. & Lee, M. Y. Cigarette smoke-induced reactive oxygen species formation: a concise review. *Antioxidants* **12**(9), 1732 (2023).
43. Checa, M. et al. Cigarette smoke enhances the expression of profibrotic molecules in alveolar epithelial cells. *PLoS ONE* **11**(3), e0150383 (2016).
44. Bennet, T. J., Randhawa, A., Hua, J. & Cheung, K. C. Airway-on-a-chip: Designs and applications for lung repair and disease. *Cells* **10**(7), 1602 (2021).
45. Silva, S., Bicker, J., Falcão, A. & Fortuna, A. Air-liquid interface (ALI) impact on different respiratory cell cultures. *Eur. J. Pharm. Biopharm.* **184**, 62–82 (2023).
46. Tulen, C. B. M. et al. Dysregulated mitochondrial metabolism upon cigarette smoke exposure in various human bronchial epithelial cell models. *DMM Dis. Models Mech.* **15**(3), 049247 (2022).

47. Mondoñedo, J. R. et al. A high-throughput system for cyclic stretching of precision-cut lung slices during acute cigarette smoke extract exposure. *Front. Physiol.* **11**, 566 (2020).
48. Elmasry, S., Asfour, S., de Rivero Vaccari, J. P. & Travascio, F. Effects of tobacco smoking on the degeneration of the intervertebral disc: A finite element study. *PLoS ONE* **10**(8), e0136137 (2015).
49. Burgess, J. K., Mauad, T., Tjin, G., Karlsson, J. C. & Westergren-Thorsson, G. The extracellular matrix—The under-recognized element in lung disease?. *J. Pathol.* **240**(4), 397–409 (2016).
50. Burgstaller, G. et al. The instructive extracellular matrix of the lung: Basic composition and alterations in chronic lung disease. *Eur. Respir. J.* **50**(1), 1601805 (2017).
51. Hackett, T. L. & Osei, E. T. Modeling extracellular matrix-cell interactions in lung repair and chronic disease. *Cells* **10**(8), 2145 (2021).
52. Zamprogno, P. et al. Second-generation lung-on-a-chip with an array of stretchable alveoli made with a biological membrane. *Commun. Biol.* **4**(1), 168 (2021).
53. Mishra, A. et al. Harmful effects of nicotine. *Indian J. Med. Paediatr. Oncol.* **36**(1), 24–31 (2015).
54. Nguyen, H. M. H., Torres, J. A., Agrawal, S. & Agrawal, A. Nicotine impairs the response of lung epithelial cells to IL-22. *Mediat. Inflamm.* **2020**, 6705428 (2020).
55. Benowitz, N. L. Pharmacology of nicotine: Addiction, smoking-induced disease, and therapeutics. *Annu. Rev. Pharmacol. Toxicol.* **49**, 57–71 (2009).
56. U.S. Department of Health and Human Services. Chemistry and toxicology of cigarette smoke and biomarkers of exposure and harm. How tobacco smoke causes disease: The biology and behavioral basis for smoking-attributable disease: A report of the surgeon general. Bookshelf ID: NBK53017 (2010).
57. Chapman, F. et al. Multiple endpoint in vitro toxicity assessment of a prototype heated tobacco product indicates substantially reduced effects compared to those of combustible cigarette. *Toxicol. In Vitro* **86**, 105510 (2023).
58. Simms, L. et al. P14–13: Use of quantitative in vitro to in vivo extrapolation (QIVIVE) for the assessment of non-combustible next generation products. *Toxicol. Lett.* **384**, 1373325 (2023).
59. Wohnhaas, C. T. et al. Monocyte-derived alveolar macrophages are key drivers of smoke-induced lung inflammation and tissue remodeling. *Front. Immunol.* **15**, 1325090 (2024).
60. Hodge, S. et al. Smoking alters alveolar macrophage recognition and phagocytic ability: Implications in chronic obstructive pulmonary disease. *Am. J. Respir. Cell Mol. Biol.* **37**(6), 748–755 (2007).
61. Wang, Y. et al. Cigarette smoke attenuates phagocytic ability of macrophages through down-regulating Milk fat globule-EGF factor 8 (MFG-E8) expressions. *Sci. Rep.* **7**, 42642 (2017).
62. Lea, S. et al. The effect of peroxisome proliferatoractivated receptor-c ligands on in vitro and in vivo models of COPD. *Eur. Respir. J.* **43**(2), 409–420 (2014).
63. Salah, B. et al. Effect of cigarette smoke on the proliferation, viability, gene expression, and cellular functions of adipose-derived mesenchymal stem cells from smoking and non-smoking donors. *Biology Open.* **13**(12), 061665 (2024).
64. Yin, Y., Hou, G., Li, E., Wang, Q. & Kang, J. PPAR Gamma agonists regulate tobacco smoke-induced toll like receptor 4 expression in alveolar macrophages. *Respir. Res.* **15**(1), 28 (2014).
65. Lakshmi, S. P. et al. Down-regulated peroxisome proliferator-activated receptor γ (PPARγ) in lung epithelial cells promotes a PPARγ agonist-reversible proinflammatory phenotype in chronic obstructive pulmonary disease (COPD). *J. Biol. Chem.* **289**(10), 6383–6393 (2014).
66. Kim, J.-L., Koca, H. K., Viklund, E. & Olin, A.-C. How does smoking influence major phospholipids and proteins in lung surfactant? **54**(63), 4265 (2019).
67. Stenger, P. C. et al. Environmental tobacco smoke effects on lung surfactant film organization. *Biochim. Biophys. Acta Biomembr.* **1788**(2), 358–370 (2009).
68. Takamiya, R. et al. Disruption of the structural and functional features of surfactant protein A by acrolein in cigarette smoke. *Sci. Rep.* **7**(1), 8304 (2017).
69. Garavaglia, M. L. et al. Molecular impact of conventional and electronic cigarettes on pulmonary surfactant. *Int. J. Mol. Sci.* **24**(14), 11702 (2023).
70. Scott, J. E. The pulmonary surfactant: impact of tobacco smoke and related compounds on surfactant and lung development. *Tob. Induc. Dis.* **2**(1), 3–25 (2004).
71. Hobi, N., Ravasio, A. & Haller, T. Interfacial stress affects rat alveolar type II cell signaling and gene expression. *Am. J. Physiol. Lung Cell. Mol. Physiol.* **303**(2), L117–L129 (2012).
72. Lopez-Rodriguez, E., Pascual, A., Arroyo, R., Floros, J. & Perez-Gil, J. Human pulmonary surfactant protein SP-A1 provides maximal efficiency of lung interfacial films. *Biophys. J.* **111**(3), 524–536 (2016).
73. Radiom, M. et al. Pulmonary surfactant inhibition of nanoparticle uptake by alveolar epithelial cells. *Sci. Rep.* **10**(1), 19436 (2020).
74. Ravasio, A. et al. Interfacial sensing by alveolar type II cells: A new concept in lung physiology?. *Am. J. Phys. Cell Physiol.* **300**(6), C1456–C1465 (2011).
75. Machado, D. F. et al. The administration of surfactant decreased oxidative stress in lungs of mice exposed to cigarette smoke. *Int. Immunopharmacol.* **54**, 275–279 (2017).
76. Caruso, G. et al. Lung surfactant decreases biochemical alterations and oxidative stress induced by a sub-toxic concentration of carbon nanoparticles in alveolar epithelial and microglial cells. *Int. J. Mol. Sci.* **22**(5), 2694 (2021).
77. Lu, Q., Gottlieb, E. & Rounds, S. Effects of cigarette smoke on pulmonary endothelial cells. *Am. J. Physiol. Lung Cell. Mol. Physiol.* **314**(5), L743–L756 (2018).
78. Iskandar, A. R. et al. Impact assessment of cigarette smoke exposure on organotypic bronchial epithelial tissue cultures: A comparison of mono-culture and coculture model containing fibroblasts. *Toxicol. Sci.* **147**(1), 207–221 (2015).
79. Milara, J., Peiró, T., Serrano, A. & Cortijo, J. Epithelial to mesenchymal transition is increased in patients with COPD and induced by cigarette smoke. *Thorax* **68**(5), 410–420 (2013).
80. Xu, H. et al. Exosomal microRNA-21 derived from bronchial epithelial cells is involved in aberrant epithelium-fibroblast crosstalk in COPD induced by cigarette smoking. *Theranostics* **8**(19), 5419–5433 (2018).

Acknowledgements

We gratefully acknowledge the financial support from Eurostars (project Nr. AIM4DOC). The authors extend their heartfelt thanks to Dr. Nuria Roldan and Lea Lara de Maddalena for their invaluable assistance in managing this study. We also appreciate the contributions of Frank Dittrich and Abhishek Malik from Vitrocell for their outstanding technical support. Additionally, we highly appreciate the knowledge and support of Prof. Dr. Claus-Michael Lehr and Dr. Clementine Richter from the Helmholtz Center for Infection Research, Saarbrücken, Germany, in the AIM4DOC project.

Author contributions

AS, NH, and OG conceived and developed the overall pipeline of this study. SS, AD and NG performed cell cul-

ture experiments, assisted other authors with experiments and/or data management. AS collected and analyzed the data and wrote the manuscript. HOW, MH and AH assisted in technical validation of the CFAX12 system. KŽ and VV performed all LC–MS/MS studies. AnjH and PK conducted the flow cytometry experiments and data analysis. PO and JPG provided SOPs and helped with the surfactant experiments. JS and TK provided inputs in their respective field of expertise. NH and OG contributed to the interpretation of the data and reviewed the manuscript. All authors provided feedback and approved the submitted version.

Declarations

Competing interests

OG and NH hold equity in AlveoliX, NH in Alexis Technologies. AH and NH are employed by AlveoliX. AS, SS, AD and NG are employed by Alexis Technologies. HOW, MH and TK are employed by VITROCELL Systems GmbH. VV declares that her spouse is employed by Philip Morris International. The remaining authors declare that the research was conducted without any commercial or financial relationships that could be construed as a potential conflict of interest.

Additional information

Supplementary Information The online version contains supplementary material available at https://doi.org/10.1038/s41598-025-00438-z.

Correspondence and requests for materials should be addressed to A.S. or O.T.G.

Reprints and permissions information is available at www.nature.com/reprints.

Publisher's note Springer Nature remains neutral with regard to jurisdictional claims in published maps and institutional affiliations.